Optimising the value of a CO_2 Water-Alternating-Gas injection project under geological and economic uncertainties using an improved artificial neural network.

P. Ogbeiwi [1,*], K. D. Stephen [1]

[1] Institute of Geoenergy Engineering, Heriot-Watt University, Edinburgh, UK.
* Corresponding author; email: prejohn73@yahoo.com; po20@hw.ac.uk

This manuscript has been submitted for publication in **Computational Geosciences**. Please note that the manuscript is undergoing peer review and is yet to be formally accepted for publication. Subsequent versions of this manuscript may have slightly different content. Please feel free to contact the corresponding author; we welcome feedback

Abstract

The numerical simulations required for the robust optimisation of the alternating injection of water and CO2 in hydrocarbon reservoirs are computationally expensive due to engineering, geological, and economic uncertainties. Using approximation models of the desired objective function(s) can significantly decrease the cost associated with the optimisation routines while providing an adequate parameter space sampling for the input variables/ uncertainties. In this study, we optimised the value of a water-alternating-gas injection project in a Niger-Delta oil reservoir by applying the Markowitz classical theory to a suitable approximation model of the objective function. Our robust optimisation methodology incorporated significant geological and economic uncertainties, such as uncertainties due to upscaling the reservoir model, and those due to the lack of other relevant geological and economic data, to the optimisation routine to create better operating strategies for the project that are risk quantified. To compute the objective function, we applied a new economic model for the CO2 sequestration processes in the Niger Delta hydrocarbon basin. The result showed that an NPV of at least 65.98 million USD was derived from the project depending on the engineer's or user's confidence level. Although this result was 63.84% lesser than the solution of the nominal optimisation (182.46 million USD), it was more realistic. Overall, the applicability of proxy models to robust optimisation routines was demonstrated, and investment decisions that included uncertainties were made.

1 Introduction

Oil recovery by water-alternating-gas (WAG) injection is highly dependent on a combination of the various engineering, economic and geological parameters that determine the performance of the injection process. Numerical simulations are important in investigating the performance of WAG injection in oil reservoirs as they can consider the numerous engineering and geological uncertainties [1]. They can be used to search the parameter space, determine the relationships between parameters, and optimise the recovery process's performance. However, using numerical simulations to analyse the performance of a WAG injection can be computationally expensive because many simulation runs are required due to the numerous uncertainties that must be considered and the large number of grid cells used in the simulation models. Therefore, it is not always practical to set up and evaluate the performance of WAG using reservoir simulation models because of the associated complexities and computational expenses. This process can, however, be simplified by approximating the desired numerical simulation output(s) such as incremental oil recovery [2], CO_2 storage [3], gas utilisation factor [4], water production [5], or project life cycle [6] with a proxy function.

In this study, we performed the robust optimisation of the value of the WAG injection project in the five-spot pilot model of the case study reservoir under geological and economic uncertainties. We applied the Latin Hypercube Design (LHD) to create the designs of the engineering, geological and economic parameters needed to calculate the objective function. Artificial intelligence was then applied to construct the proxy models of NPV response. Further improvements to the derived neural network were then made, and the Markowitz classical theory was applied to the resulting NN model to perform the robust optimisation routine. The non-dominated sorting algorithm was then applied to generate the Pareto fronts needed to rank the optimality of the resulting solutions.

2 Theoretical Background

2.1. Optimisation under Uncertainty: Markowitz classical theory and the Efficient Frontier

In this study, the Markovitz classical theory was applied for the robust optimisation of the WAG project under uncertainty. The theory is a method of optimising under uncertainty (Markowitz, 1952, as cited by Bailey and Couet, 2005). An extensive review of this approach and its advantages was done by [9].

To apply this theory, we categorised the decision variables that were within the engineer's or optimiser's control from those that were not within our control, such as the geological and economic uncertainties. We termed the latter set of variables as the optimisation process's uncertainties. The response of the system can be described as follows:

$$f = f(\underline{\alpha}, \underline{\beta}) \tag{1}$$

where $\alpha = \{\underline{\alpha}_1, \underline{\alpha}_2, \underline{\alpha}_3, \dots, \underline{\alpha}_N\}$ and $\beta = \{\underline{\beta}_1, \underline{\beta}_2, \underline{\beta}_3, \dots, \underline{\beta}_N\}$ represent the sets of process' design variables and uncertainties, which affect the system respectively. Arithmetically, a probability distribution function can be applied to represent the distribution of the uncertainties, and the optimiser could decide to use n samples to represent this [8]. In a system having m uncertainties, $N = n^m$ realisations of the system are needed to sample these uncertainties.

For the N realisations, the mean and standard deviation are given as:

$$\mu(\alpha) = \frac{1}{N}\sum_{i=1}^{N} f_i \tag{2}$$

and

$$\sigma(\alpha) = \sqrt{\frac{1}{N}\sum_{i=1}^{N}(f_i - \mu(a))^2} \tag{3}$$

An efficient frontier can be obtained by plotting $\mu(\alpha)$ against $\sigma(\alpha)$. This is the set of points which have a higher μ than any other with the same or lower σ, and lower σ than any other with the same or higher μ. It optimises μ for a given σ and optimises σ for a given μ (Markowitz, 1952).

A mean-variance approach is typically applied to optimize f, which takes the form (Couet et al., 2000):

$$F_\lambda = \mu(\alpha) - \lambda\sigma(\alpha) \tag{4}$$

where λ is the risk-aversion factor which specifies the optimiser's aversion to risk (or uncertainty). Different $\lambda \geq 0$ can be used to determine this frontier which is equal to the points that maximise the utility or objective function (Bailey and Couet, 2005). When a higher value of λ is selected, it describes a higher risk aversion (or lesser risk tolerance) and greater confidence. When the samples have a normal distribution, λ of 0, 1, 2, 3 and 4 corresponds to confidence levels of 50.00, 84.13, 97.72 and 99.99 %, respectively [11].

In the present study, we systematically selected the five confidence levels to account for a wide range of risk aversion in the optimisation under uncertainty routine as stipulated by Bailey and Couet (2005). A search algorithm, the genetic algorithm (GA), was applied to locate the maximum F_λ for a specified λ. This process was then repeated for other values of confidence levels. An extensive review of the GA and its suitability for robust optimisation under uncertainty has been discussed by Ogbeiwi et al., (2020). The resulting models can be plotted on the mean vs standard deviation (or variance) plot, and the optimal models for each λ will form a convex hull known as the efficient frontier [8]. Using this approach, the "risks" (related to the uncertainties) can be correlated

with the potential rewards. Decisions having low rewards can be detected and ignored based on the risk allowing us to account for uncertainties/risks while ascertaining the benefits of various decisions.

In the optimisation routine, many independent computations of the reservoir model are required, and these have a high CPU cost. As shown by Ogbeiwi et al., (2020), using suitable approximation models effectively mitigates the high computational cost associated with applying the Markowitz classical theory in robust optimisation routines. This is done by applying data-driven adaptive proxy modelling methods to build a surrogate model of the desired output based on a relatively small amount of full-physics simulations. The resulting approximation model correlates the engineering design variables and the uncertain input parameters to the desired response, and it can be applied for fast simulations, optimisation and decision-making under uncertainty [13].

2.2. Experimental Design (ED) and Surrogate Modelling

Experimental designs and data-driven proxy modelling has been commonly employed in enhanced oil recovery (EOR) where they are used to create surrogates for the full-physics reservoir model. Common surrogate modelling approaches include polynomial regression (Ampomah et al., 2016; Agada et al., 2017; Dalton et al., 2017; Ogbeiwi et al., 2020), Kernel methods such as the Radial Basis Function (RBF) [17], multivariate adaptive regression splines (MARS) [18], Kriging techniques [19], Polynomial Chaos Expansion (PCE) [20]–[22], and artificial neural networks (Costa et al., 2014; Foroud et al., 2014; Negash et al., 2017; Ampomah et al., 2017; Golzari et al., 2015; Maschio and Schiozer, 2015; Jang et al., 2018; Villarrubia et al., 2018; Jiang et al., 2020; You et al., 2020).

These methods use complicated mathematical relationships between simulator input and output to mimic physical systems and swiftly replicate the desired output patterns. Jin et al., (2001) compared the performance of several surrogate modelling techniques based on multiple criteria, including robustness, accuracy, efficiency, transparency, and conceptual simplicity. Their results showed the dependence of the performance of proxy models on the sampling technique used to generate designs for constructing them. An extensive review of experimental design and proxy modelling techniques and their suitability for robust optimisation problems has also been performed by Ogbeiwi et al., (2020).

In this study, we applied an artificial neural network to construct approximation models of the desired objective function. Artificial intelligence has emerged as a prominent tool for oil and gas problems and has received many successful applications, particularly in reservoir performance optimisation (Ampomah et al., 2017; Golzari et al., 2015; Maschio and Schiozer, 2015; Jang et al., 2018; Villarrubia et al., 2018; Jiang et al., 2020; You et al., 2020). The Latin-Hypercube Design was applied to design the simulation experiments regarding the engineering, geological and economic parameters needed to calculate the objective function. The Latin-Hypercube design is a pseudo-Monte Carlo sampling design and has received many applications in oil and gas reservoir modelling and optimisation problems [21], [34]–[38].

Artificial Neural Networks (ANNs) are information processing systems approximating biological neural network system. They comprise of artificial neurons that are highly interconnected and serve as processors. They are characterised by the number of neurons and layers and their connectivity [24]. The correlations between the inputs and outputs are modelled using the neurons and their connectivity weights. In this study, the ANN training task was done by setting the network's weights and biases to approximate the NPV responses of the full-physics numerical simulation models.

The predictability and quality of the proxy model can be measured using different error metrics. In this study, we applied the R^2 Goodness of fit to verify the quality of our surrogate models (Ogbeiwi et al., 2020). The R^2 goodness of fit is given as:

$$R^2 = 1 - \frac{SS_{res}}{SS_{tot}} \quad (5)$$

where $SS_{tot} = \sum_{i=1}^{N_d}[|{y_t}^{(i)} - \bar{y}_t|]^2$, ${y_t}^{(i)}$ = experimental values, ($\bar{y}_t$)= mean of the experimental values, and $SS_{res} = \sum_{i=1}^{N_d}[|e^{(i)}|]^2$, and $e^{(i)} = \frac{\hat{y}_t{}^{(i)} - {y_t}^{(i)}}{{y_t}^{(i)}}$.

2.3 The optimisation objective function: An economic model for CO_2 EOR and/or storage processes in the Niger-Delta

To compute the objective function, we developed a new economic model for CO_2 EOR and storage processes in the Niger-Delta hydrocarbon basin and applied this to compute the objective function. This requires the establishment of the net annual cashflow profile which was given as the annual cash inflow less outflow, plus the "allowable" fixed assets' depreciation. The following relationship was used to compute the annual cash flow [40]:

$$NCF = R - C_{CAPEX} - C_{OPEX} - C_{ROY} - C_{TAX} - C_{CO2} \quad (6)$$

where R is the gross revenue, C_{CAPEX}, C_{OPEX}, C_{ROY}, and C_{TAX} are the capital expenditure, operating expenditure, royalty, and tax, respectively, and C_{CO2} is a "fine" for any fugitive carbon emissions. The gross revenue R comprised cash receipts from oil and gas sales and any credits accrued due to the secure carbon storage.

The royalty and tax expenditures, C_{ROY} and C_{TAX} can be calculated as:

$$C_{ROY} = r_r R', \quad (7)$$

$$C_{TAX} = r_t(R - C_{ROY} - C_{OPEX} - C_{DEP}) \quad (8)$$

where r_r and r_t are royalty and tax rates, respectively. C_{DEP}= depreciation, and R' = gross revenue less carbon credits. These estimates are made on an annual basis. The royalty and tax disbursements are government receipts due to the fiscal policy of Nigeria (Lawal, 2011; Echendu and Iledare, 2016).

The NPV objective function was estimated from the NCF as:

$$NPV = \sum_{i=1}^{n} \frac{NCF}{(1+r_D)^i} \quad (9)$$

where r_D is the discount rate which amortises the capital expenditure over the lifecycle of the project [43]. The analyses were carried out for 10 years of CO_2 injection.

2.3.1. The Capital Expenditure (CAPEX) and Operating Expenditure (OPEX) Components

The capital cost relates to wells, flowlines and processing facilities. Given the existence of flowing producers and injectors, and existing surface facilities in the reservoir, the CAPEX also included the cost of converting the existing water injection facilities to CO_2 flooding facilities and vice-versa [44]. Since the reservoir was a mature oil field, the cost of drilling and completing additional injectors and producers and their corresponding surface facilities were also included. In summary, the CAPEX considered included the workover cost of existing producers and injectors, pattern production and injection equipment, CO_2 processing equipment, and drilling and completing new wells. Provisions were also made for contingency and decommissioning costs.

The OPEX of the project included typical daily expenditure and other consumables expenses such as gas injection, oil treatment, CH_4 treatment, water handling, and surface and subsurface facilities maintenance costs. After the

breakthrough of CO_2 at the production wells, any produced CO_2 can be extracted and reused with the purchased CO_2 for injection.

The total annual operating cost was given as:

$$C_{OPEX} = \text{O\&M}^{t}_{annual} = \text{O\&M}^{t}_{daily} + \text{O\&M}^{t}_{cons} + \text{O\&M}^{t}_{sur} + \text{O\&M}^{t}_{subsur} + \text{C}^{t}_{rec} + \text{C}^{t}_{CO_2} + \text{C}^{t}_{Water} \quad (10)$$

A summary of the important components of the CAPEX and OPEX, and the presumed reference values is shown in Tables 1 and 2, respectively.

Table 1: Components of Operating Expenditure

Variable	Value	Comments/ References
Fixed OPEX (%)	5	Fixed OPEX is 5% of CAPEX (Lawal, 2011; Wei et al., 2015)

Variable OPEX		
Gas Injection ($/ MMscf)	580	[46], [47]
Carbon Capture, ($/ MMscf)	1600	[47], [48].
CO_2 Compression Cost, ($/ t CO_2)	The mean cost of 13USD/t for 1Bar of CO_2 and 1USD/t for high pressured gas from a pipeline terminal were applied.	Wei et al., (2015)
CH_4 Treatment, ($/ MMscf)	400	A value of 20% of sale gas price was assumed Wei et al., (2015).
Fluid Handling/ Treatment, ($ /stb)	1 for oil and water pumping, and 12 for oil treatment.	[49]
Water Compression and Injection, ($ /m^3)	1.2 for a WAG process regardless of pressure difference	Anthony and Mohan, (2010); Wei et al., (2015)
CO_2 recycling cost, ($/ t CO_2)	$C_{rec} = 23.66 \cdot Q$	Wei et al., (2015); Tayari et al., (2015)
Daily and Consumables O & M Costs, $/annum	Daily O&M = N_{well} x 7596. Cons. O&M = N_{well} x 20,295	Wei et al., (2015)
O & M cost for well facilities, $/annum	$O\&M_{sur} = N_{well}$ x 15420 x $[(d/(280 \times N_{well}))^{0.5} + 5000]$; $O\&M_{subsur} = N_{well} \cdot [5669 \cdot (d/1219)]$	Wei et al., (2015)

Table 2: CAPEX Components

Variable	Value	Comments/ References
Drilling and Completions		

Number of new injectors	1	-
Number of new producers	2	-
Cost (10^6 $ / well)	1.5	Tayari et al., (2015)
Surface Pipelines		
Number of injection lines	1	One flowline per injector
Number of new production lines	2	One flowline per producer
Length per line (km)	1	
Cost (10^6 $ / well)	0.5	Tayari et al., (2015); Cremon et al., (2020)
Processing Facilities		
Peak water rate (10^3 stb/d)	3	Based on the secondary waterflood (Ogbeiwi et al., 2020b)
Peak liquid rate (10^3 stb/d)	5	Based on the secondary waterflood (Ogbeiwi et al., 2020)
Cost of liquid facilities (10^6 $ / 10^3stb liquid)	1.9	Wang et al., (2018)
CO_2 Capture and Compression Facilities		
Peak gas rate (10^6 scf/d)	1	This rate will decrease across the project's lifecycle since produced CO_2 will be recycled.
Peak CO_2 injection rate (10^6 scf/d)	1	This rate is dependent on the gas cycle time of CO_2 injection.
Unit cost of capture (10^6 $ / 10^6scf)	13	[54], [55].
Unit compression cost ($ mln / MMscf)	1.3	Gaspar Ravagnani et al., (2009)
Other Components		
CAPEX contingency (%)	10	Assumption [40]
Decommissioning cost (% of CAPEX)	25	[56], [57]
CAPEX phasing (% / year)	100	CAPEX spending calculated for the first year.

2.3.2. Revenues and Penalties

The sources of revenue considered include revenue from the sale of the recovered hydrocarbon and that obtained due to the volume of CO_2 sequestered, known as carbon credit. In the economic model, penalties were incurred for any fugitive emission of CO_2. The reference values are shown in Table 3.

Table 3: Revenue and Penalty Rates

Item	Rate	Comments/ References
Oil Price, $/stb	70	Bloomberg, (2022)
CH_4 price, $/Mscf	2	Mokhtari et al., (2016); Hill et al., (2013)
Carbon Credit, $/ton CO_2	16	Mokhtari et al., (2016)
Carbon Penalty, $/ton CO_2	60	IHS MARKIT, (2016)

2.3.3. Fiscal Policy

The Nigerian government receives three taxes for operations in its upstream petroleum sector, namely the corporate tax, Petroleum Technology Development Fund (PTDF) tax, and Tertiary Education Trust Fund (TETFund) tax [55]. The reference values of these terms are shown in Table 4.

Table 4: Components of Fiscal Terms

Item	Rate	Comments/ References
Corporate tax, %	30	CITA, (2004); PPT, (1990)
PTDF Tax, %	3	PTDF, (1990)
TETFund Tax, %	2	ETF, (1993)
Depreciation, %	20	NIPC, (2010)
Royalty, %	8	PPT, (1990)
Discount Rate, %	10	Yang et al., (2007)

In the Niger Delta, the royalty rate depends on the location of the reservoir, the type and volumes of hydrocarbons produced, and the price of oil (Echendu and Iledare, 2016; PIB, 2009). For offshore basins to which the case study reservoir belongs, the royalty is 8.0% (Onwuka et al., 2012; Echendu and Iledare, 2016). For the sake of simplicity, we also assumed this value as the royalties applied to the prices and volume of hydrocarbons produced. We also applied the straight-line depreciation of assets stipulated by the Nigerian government (NIPC, 2010) and equally depreciated the CAPEX elements over the first three years of incurring the expenditure.

3 Methodology

3.1 The Case study: Field Description

The simulations were run using the five-spot pilot sector model extracted from a calibrated full-field model of an under-saturated oil reservoir in the Niger-Delta, as shown in Fig. 1. The vertical and horizontal grid resolutions and the original rock and fluid properties were retained in the pilot model. The model consists of 9 x 7 x 25 grid cells with an average dimension of 330 x 330 x 2.5ft. The pilot WAG injection was then performed using an inverted five-spot pattern. To ensure consistency, the pressure field, phase saturations and other properties were initialised directly from the results of the full-field simulations at the end of the secondary waterflooding of the reservoir.

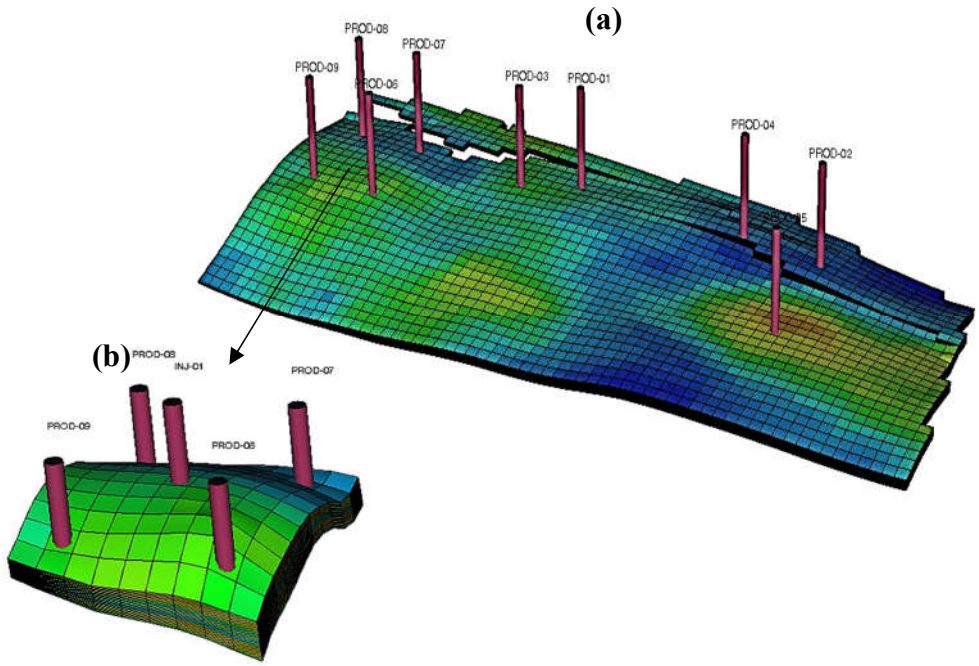

Fig. 1: The five-spot pilot sector model (a) was extracted from the calibrated full-field model (b).

Arinkoola et al., (2016) and Ogbeiwi et al., (2020) presented the properties of the reservoir model and descriptions of the history matching procedure and primary and secondary production schemes. The compositional fluid model was presented by Ogbeiwi and Stephen, (2021). The minimum miscibility pressure (MMP) of the reservoir oil with CO_2 was computed using the Glasø correlation (Glasø, 1985 as cited by Ahmadi et al., 2017) of the Schlumberger PVTi software 2019 as 80.7 bars (1170.46 psia) (ECLIPSE, 2019).

3.2. Description of Key Uncertainties

3.2.1. Economic Uncertainties

Eight economic parameters were considered uncertain regarding the project's net present value (NPV). Table 5 shows these parameters and the range of uncertainty considered. The uncertainties in the offshore Niger Delta hydrocarbon province's tax regimes and fiscal policy were ignored since these are government policies and are not prone to changes like other variables.

Table 5: Economic Uncertainties and their ranges.

Economic Variable	Low (-1)	Median (0)	High (+1)
Oil Price, $/stb	50	70	80
Discount Rate, %	5	10	15
Carbon Credit, $/ton CO_2	0	10	20
Gas (CH_4) price, $/MMscf	0	2000	2500
Change in CO_2 recycling cost	0	10	30
CO_2 injection cost, $/MMscf	580	1000	2000
Change in unit OPEX cost, %	0	10	30
Increase in CAPEX, %	0	10	30

According to the Annual Energy Outlook (AEO), the West Texas Intermediate (WTI) oil price rose from $60 per barrel (in 2019 dollars) to $100 in 2022. However, a low price of $50 and a high price of $80 were applied to account for oil price volatility. For deterministic analysis, an average price of $70, the average crude oil price between 2019 and 2022, was assumed.

The range of uncertainty of other parameters was based on the existing economics of the hydrocarbon industry of Nigeria and other assumptions as listed in Tables 1, 2 and 3. For example, given the lack of CO_2 EOR projects in the Niger-Delta, the absence of carbon credits was assumed as the worst-case scenario, while revenue of $20/tonne of CO_2 stored was assumed as the best-case. Also, given the lack of an ever-ready market to purchase produced CH_4, we assumed that in the worst-case scenario, there would be no revenue from the sales of the produced gas, and all of it would be converted to CO_2 for injection. To account for inflation, we assume a maximum change of 30% to the cost of CO_2 recycling, unit operations, and capital expenditure (CAPEX).

3.2.2 Description of the Well Controls and Engineering Variables

Different parameters, such as CO_2 slug size, WAG ratio, gas injection rate, bottom-hole pressures (BHPs) affect the performance of WAG floods. For example, the BHPs of the injectors and producers are significant parameters during miscible CO_2 flooding since CO_2 injected into the reservoir is required to remain at or above its miscibility pressure (MMP) for optimal oil recovery [73]. Table 6 shows the design parameters utilised in this study and the range of the sampling space considered for each parameter.

Table 6: Engineering design parameters and their ranges.

Design Variable	Low (-1)	Median (0)	High (+1)
Gas Cycle Time (months)	4	6	10
Water Cycle Time (months)	2	4	6
Target Oil Production Rate (for each producer) (stb/day)	500	750	1000
Target CO_2 injection rate (scf/day)	11600	16800	22400
Maximum Injector BHP (psia)	2000	2500	3000
Maximum Production Well BHP (psia)	1150	1300	1400

3.2.3 Geological Uncertainties

The geological uncertainties assessed include relative permeability hysteresis parameters, layering within the reservoir, micro- and macro-scale physical instabilities, and uncertainties in the absolute permeability and porosity within the reservoir.

Relative Permeability Hysteresis: Numerous studies such as those by Spiteri and Juanes, (2006); Pham et al., (2011); Shahverdi and Sohrabi, (2015) and Assef et al., (2019) indicated that the relative permeability hysteresis has a significant impact on the retention and displacement of fluids in the porous media during WAG floods. To understand the effects of hysteresis on the project's performance, some relative permeability hysteresis quantities, such as the Land trapping parameter C, and secondary drainage reduction factor α, were regarded as uncertainties in this study.

Reservoir Stratification: Due to the lack of well logging and core data for the wells around the pilot sector model, uncertainty of the layering/ stratification in the pilot model was assumed. A cross-sectional view of the model reveals five distinct stratified permeability layers containing two highly productive formations (Fig. 2). The layers within the reservoir rock were identified to be communicating from the history-matching by Arinkoola et al., (2016). We accounted for this uncertainty by considering variations in the permeability, porosity, and fluid saturation distributions within the layers within the pilot model. These were given as L1, L2, and L3, representing three cases of stratification uncertainty.

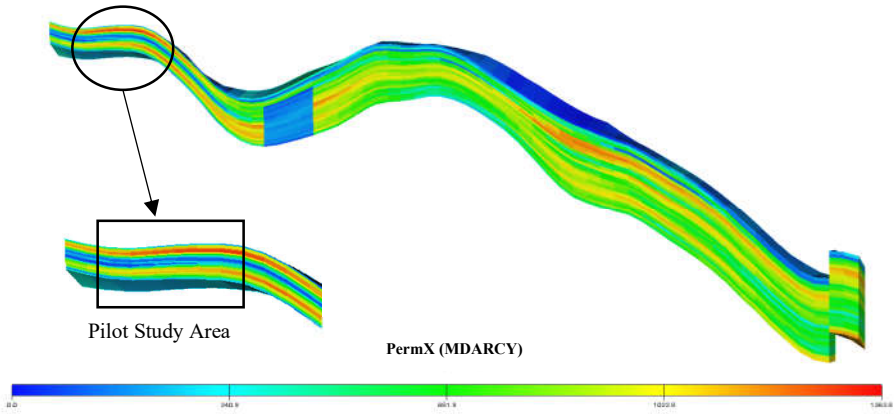

Fig. 2: A cross-section of the full reservoir model showing the presence of permeability strata.

Grid Coarsening/ Upscaling: Ogbeiwi and Stephen, (2021) indicated that small-scale physical instabilities such as viscous fingering, permeability heterogeneity, and physical diffusion must be incorporated into the coarse-scale simulation of CO_2-enhanced oil recovery for more accurate results. Their results showed that the calculated pseudo-relative permeability functions are negligible compared to efficiently tuned transport coefficients. Hence, we accounted for any uncertainties due to the coarsening of the grids by incorporating uncertainties of transport coefficients.

Other Geological Uncertainties Arinkoola et al., (2016) and Ogbeiwi et al., (2020) presented other significant uncertainties, such as vertical permeability, porosity, and horizontal permeability, that influence the drainage and injection processes from the case study reservoir. The distributions of these uncertainties were relatively unknown and were modified to calibrate the reservoir's pressure and saturation history.

In summary, this study considers seven geological quantities uncertain, as shown in Table 7.

Table 7: Geological Uncertainties and their ranges.

Design Variable	Low (-1)	Median (0)	High (+1)
Land trapping parameter, $\boldsymbol{C}$	0.2	1	2
Secondary drainage reduction factor, $\boldsymbol{\alpha}$	0.1	0.2	1.0
Layering	L1	L2	L3
Transport Coefficient	1	2.5	4
Global porosity	0.9	1	1.1
Vertical permeability	0.5	1	6
Horizontal permeability	0.57	1	1.29

3.3. Sensitivity Analysis

The Plackett-Burman design was applied to generate the simulation runs to assess the effects of the engineering design variables, geological uncertainties, and economic uncertainties on the objective function. These effects were represented as the percentage contribution of each variable to changes in the objective function [69]. This was given as follows:

$$\%\ contribution = \frac{|Y_{i,max} - Y_{i,min}|}{\Sigma|Y_{i,max} - Y_{i,min}|} \times 100\% \quad (11)$$

where $Y_{i,max}$ and $Y_{i,min}$ are the maximum and minimum values of the objective function(s) evaluated for the minimum and maximum values of each variable i, respectively. The denominator represents the sum of the numerator for all the variables.

The results of the preliminary screening analysis of the economic uncertainties are presented in Fig. 3. The price of the produced oil was the most significant economic uncertainty, and changes to it resulted in more than 60% changes in the project's value. Other significant economic uncertainties with more than 5% contribution include the cost of CO_2 injection and the discount rate.

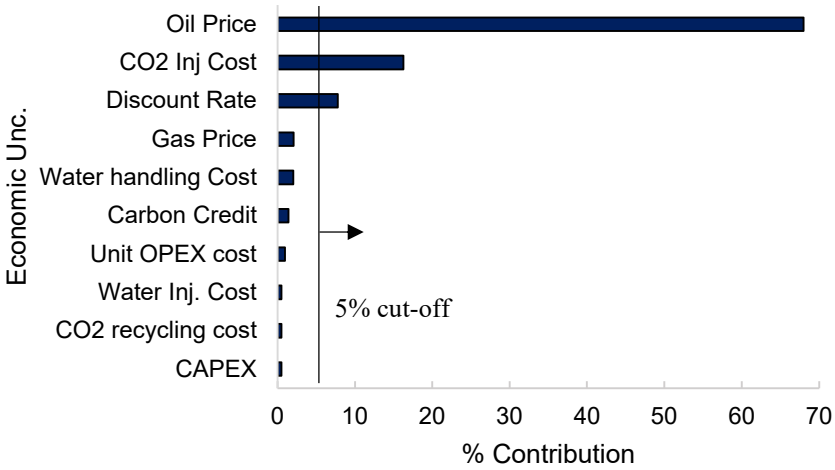

Fig. 3: Pareto charts showing the key economic uncertainties impacting NPV.

The sensitivities of the economic uncertainties to the NPV response were assessed by varying one parameter at a time and are presented in Fig. 4. Varying the oil price from 50 – 80 USD/stb resulted in a 75.83% increase in the NPV from 82.83 to 145.64 million USD. Also, a change in the operating cost of CO_2 injection resulted in a 16.3% decrease in the value of the project from 125.63 to 102.84 million USD. The change in capital expenditure had the least effect on the NPV, resulting in only a 0.5% decrease in the value of the project.

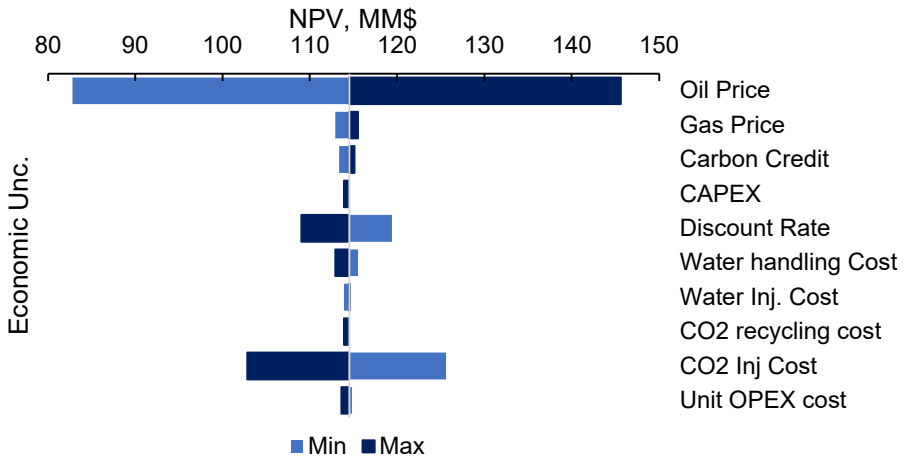

Fig. 4: Sensitivities of the economic uncertainties on the NPV response.

3.3.1 Engineering Variables and Geological Uncertainties

The net cash flow must be positive for the WAG injection process to be commercially viable, i.e., NCF > 0. Since the revenues were incurred from the volumes of hydrocarbons produced and CO_2 stored, which are functions of the engineering and reservoir parameters, it was also necessary to assess the effects of the engineering control variables and the geological uncertainties on the value of the project. The results of the sensitivity analyses of the engineering and geological uncertainties are shown in Fig.s 5 (a) and (b), respectively.

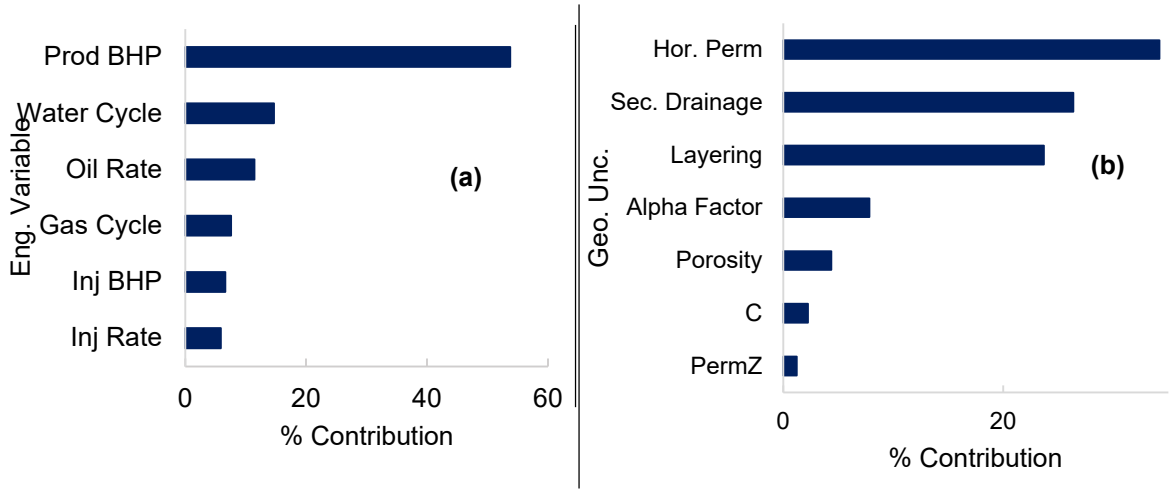

Fig. 5: Pareto charts showing the key (a) engineering control variables and (b) geological uncertainties impacting the NPV response.

Overall, the bottom-hole pressure of the producers (which determines the miscibility of the flood), the length of the water cycle time (the sweep conformance of the flooding process), and the target oil production rate were the three most important technical parameters as presented by Fig. 5(a). On the other hand, the global horizontal permeability, the secondary drainage factor, the level of stratification of the reservoir and the transport coefficients were the most important geological uncertainties.

The sensitivity analysis of the engineering and geological uncertainties is presented in Fig. 6. When the BHP of the producers was changed from the minimum to the maximum values, the NPV of the project decreased from 222.94 to 148.48 million USD. Also, a change in the length of the water cycle time from 2 to 6 months resulted in an 11.57% increase in the NPV, while an increase in the target oil rate resulted in a corresponding increase of 8.93% in NPV. Conversely, the maximum CO_2 injection rate had the least effect on the NPV, resulting in only a 4.29% decrease in the value of the project.

The values of the global horizontal permeabilities had the most significant effect on the project's NPV resulting in a 68.17% increase in NPV from 59.93 to 100.77 million USD. The effects of the transport coefficients (alpha factors), layering (stratification) and the secondary drainage factor were also prominent, resulting in changes of -12.22%, +42.03 and -32.0%, respectively. The effects of other uncertainties are presented in Fig.s 6(a) and (b).

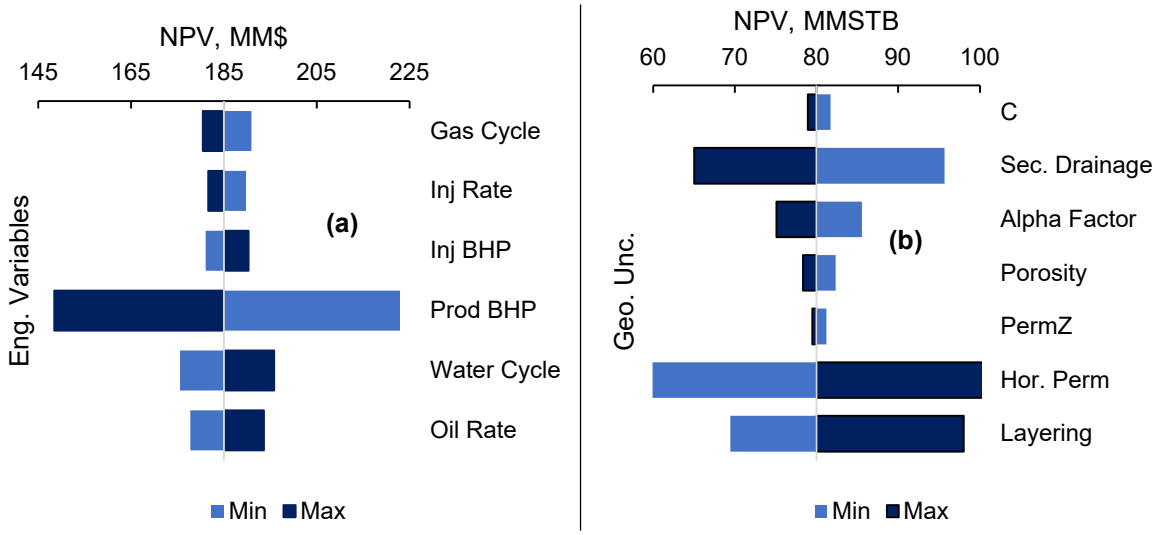

Fig. 6: Summary of the sensitivities of (a) engineering control variables (b) geological uncertainties on the NPV response.

3.4 Experimental Design and Surrogate Modelling

Including many uncertainties implies large-scale dimensionality and a higher computational expense of the investigated problem, particularly when these uncertainties have small effects on the objective function (Agada et al., 2017; Ampomah et al., 2017). Therefore, before constructing the proxy model, the sensitivity analysis results were applied to ascertain the significant parameters to be retained in the proxy modelling.

As usual, the sensitivities of the engineering, economic and geological uncertainties on the value of the WAG injection project were performed by varying one variable at a time. The significant factors include oil price, horizontal permeability, and the hysteresis parameter, the secondary drainage factor (see Fig. 7). The discount rate had the least effect on the NPV objective function. The screening results (Fig. 8) showed that the price of oil was the most important economic variable, and changes in oil prices from $50 – 80 resulted in an increase of NPV from 87.9 – 153.6 million USD. Similarly, horizontal permeability was the most significant geological parameter changing the NPV from 106.2 – 167.13 million USD. The bottom-hole pressure of the producers (Prod BHP) was the most significant engineering variable leading to a decrease of the NPV from 144.11 – 97.35 million USD for the maximum and minimum values.

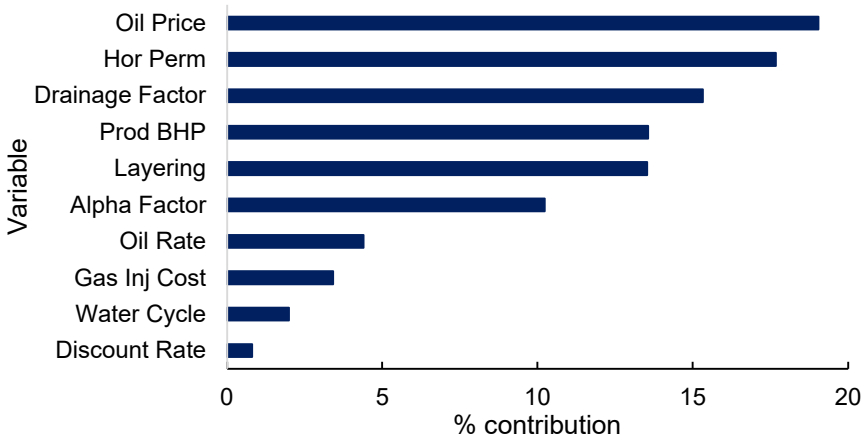

Fig. 7: Pareto charts showing the key parameters.

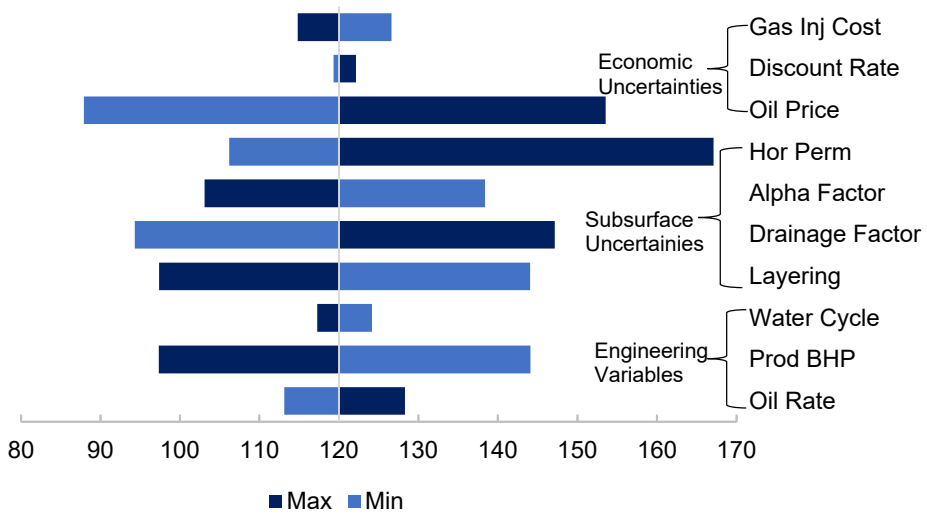

Fig. 8: Sensitivities of key parameters on the NPV response.

In summary, the engineering control variables accounted for about 20% of the changes in the NPV output, while the geological and economic uncertainties accounted for variations of approximately 57% and 23%, respectively. This shows that the optimisation problem is apt and balanced. In problems where the uncertainties are too dominant, they dominate the optimisation routine, and the optimisation of the control variables is needless since the process is out of the optimiser's control. Conversely, in the presence of negligible uncertainties, the optimisation problem is simplified, and the robust optimisation may behave like a nominal or deterministic one without uncertainties. Table 8 presents the values of surrogate model's input variables.

Table 8: Minimum, median and the maximum values of input variables.

	Variable	Minimum	Base case	Maximum
Engineering	Oil Rate (stb/day)	500	750	1000
	Maximum Producer BHP (psia)	1160	1250	1400
	Water Cycle Time (Months)	2	4	6
Geological	Secondary Drainage Factor	0.3	1.0	3.0
	Layering	L1	L2	L3
	Horizontal Permeability multiplier	0.57	1.0	1.29
	Transport Coefficient multiplier	1	2	4
Economic	Oil Price ($/stb)	50	70	80
	CO_2 injection cost ($/MMscf)	580	1000	2000
	Discount Rate (%)	5	10	15

3.4.1 Numerical Simulations, Surrogate Modelling and Testing

One hundred full-physics numerical simulations of the WAG injection scheme were performed based on a Latin-Hypercube design to compute the NPV and used to train the neural network model. The feed-forward backward propagation multi-layered neural network architecture (BPNN) implemented in MATLAB [79] was applied. The

input layer contained 12 layers (one for each input variable). The layering uncertainties were specified individually since they are categorical variables. A hidden layer containing 20 neurons was used to connect to the input layer by weights and a transfer function:

$$a_i^1 = tansig(y_i + b_i^1),\ i = 1 - 20 \quad (12)$$

$$\text{with: } y_i = \sum_{j=1}^{20} X_{ij}\,; \quad X_{ij} = X_j\,.\,w_{ij}^1 \quad (13)$$

where X_{ij} is the input parameter, w_{ij}^1 represents the weight of the j^{th} neuron of the input layer that connects with the i^{th} neuron of the hidden layer, and b_i^1 is the bias value of the i^{th} neuron in the hidden layer. A tangent-sigmoid transfer activation function was specified as follows:

$$tansig(x) = \frac{2}{1+e^{-2x}} - 1 \quad (14)$$

A sensitivity analysis informed the choices of the number of neurons and the transfer activation function. Twenty additional simulations were performed to test the accuracy of the resulting surrogate model.

3.4.2 Surrogate Modelling

An objective function, the Net Present Value (NPV) of the project at the end of 10 years of WAG injection, was developed in this study. The Latin Hypercube design was used to design 100 full-physics simulation experiments for constructing the approximation models and 20 additional simulation runs to test the constructed surrogate models. The accuracy of the proxy models was determined using the coefficient of determination (or the R^2 goodness of fit). The performances of the approximation models are compared below.

Predictions of the ANN Model

In the NN model, the backpropagation algorithm initiates the vectors of the initial weights and bias values from which the feedforward network calculates the output. The accuracy of the estimation was measured as the error between the actual NPVs and the proxy predicted NPVs. The weights and biases of the NN model are adjusted throughout the training process using the Levenberg-Marquardt algorithm. As this adjustment is carried out, a more accurate model can be typically obtained when a larger volume of data is used in the training routine. Conversely, using inadequate data for the training can result in overfitting the training data, where the model estimates the training data to a high accuracy but underperforms for the test and other data Therefore, it was necessary to use an optimal amount of training and testing data in the modelling process so that the constructed model performs optimally for all the data it was used to predict. The results of the NPV of the training data ranged from 20 – 270 MM$, while the distribution of the testing data ranged from 25 – 330 MM$, indicating a sufficient change in the parameter space, which guarantees the quality of the training and testing data.

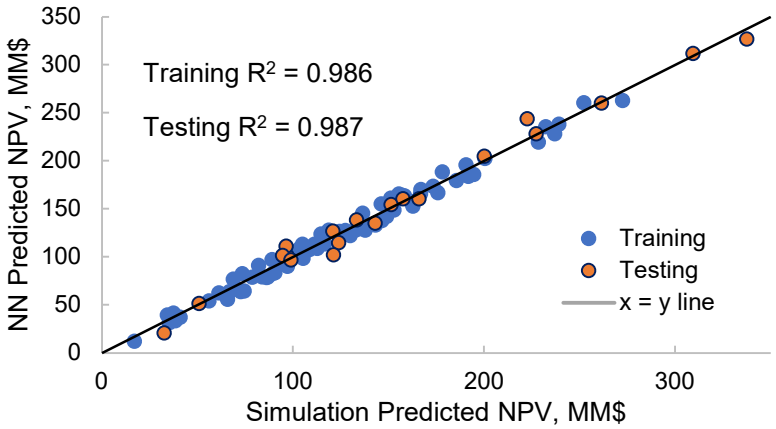

Fig. 9: Parity plot of the simulation predicted NPV values vs. the predictions of the neural network model.

The R^2 goodness of fit of the NN predicted NPV was evaluated to determine its accuracy, as shown in Fig. 9. The R^2 of the training and testing data are 0.986 and 0.987, respectively indicating that the model is valid and accurately predicts the actual simulation results.

Improving the Surrogate Model

During the construction of a data-driven surrogate, a mismatch is commonly encountered when the predictions of the data-driven proxy model are compared to the solutions of the true full-physics simulations, even for the best-performing models. The traditional approach to eliminating this mismatch is to perform an adaptive iterative update on the surrogate by adding more training data runs and testing points until a suitable match is obtained (Agada et al., 2017; Arigbe et al., 2019; Ogbeiwi et al., 2020). However, this process is often rigorous and computationally expensive because many full-physics simulations may be required to eliminate the mismatch.
To avoid this, we proposed a more efficient way to improve the surrogate model in this study. The surrogate model was improved by optimising the weights and biases of the ANN model using a GA in an approach known as the genetic algorithm-based-back-propagation artificial neural network (GA-BPNN) modelling (Chen et al., 2014). As a combined prediction-optimisation method, the algorithm offered an excellent prediction ability because it combined the inherent advantages of the neural network, such as its ability to fit non-linear data more accurately, and those of the genetic algorithm, i.e., its efficient and parallel global optimum solution searching abilities. The parameters of the GA operators are presented in Table 9.

Table 9: Genetic algorithm operators

Variable	Value
Population per generation	50
Maximum generations	50
Mutation probability	5%

The GA minimised an objective function defined as the error of the predictions of the NN proxy model represented as the root mean square error between the NPV predicted by the NN model and the numerical simulations and

stochastically searched for the optimal values of the corresponding weights and biases of the model. This method was also discovered to be computationally inexpensive and adaptable when applied to the surrogate modelling routine. The optimal solutions were then retained as the new weights and biases of the optimal NN model. The predictions of the resulting NN model are presented in Fig. 10.

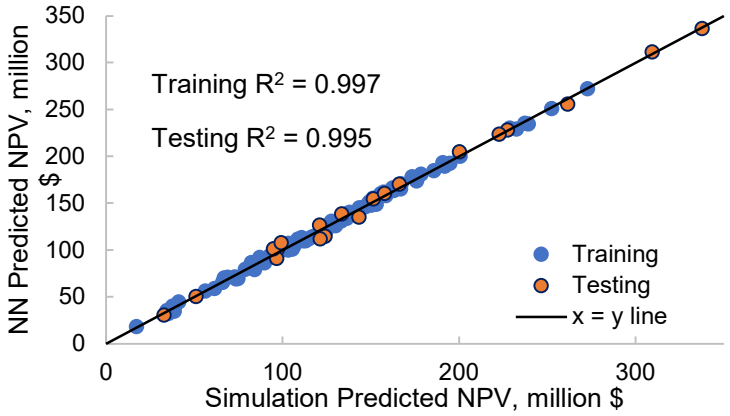

Fig. 10: Parity plot of the simulation predicted NPV values vs. the predictions of the GA-optimised, neural network models.

The optimised NN model results in better R^2 goodness of fit than the unoptimised approximation model. The R^2 of the training and testing data of the unoptimised neural network model was 0.986 and 0.987, respectively, while the R^2 of the training and testing data of the optimised neural network model was 0.997 and 0.995, respectively.

3.5 Robust Optimisation of the value of the WAG flood

A genetic optimisation algorithm, implemented in MATLAB [79] in a single objective function approach to compute the optimal control parameters for maximising the NPV of the WAG project, was applied in the optimisation routines of the WAG floods. The GA operators applied are presented in Table 9.

3.5.1. Nominal optimisation (NO)

A nominal optimisation base scenario was done for comparison, where the values of the uncertain geological and economic variables were assumed to be deterministically known and set to the median values, as presented in Tables 6 and 8.

3.5.2. Optimisation under uncertainty

In the current mean-variance optimisation problem, we applied 3000 realisations of uncertainties to adequately sample the parameter space of uncertain variables to mitigate inaccuracies in the computations of mean and standard deviation that occur when an inadequate number of samples is used in the robust optimisation routine. The objective function was given as follows:

$$\text{Maximise:} \quad F_\lambda(\underline{\alpha}) = \mu(\underline{\alpha}) - \lambda\sigma(\underline{\alpha}) \tag{15}$$

$$s.\ t.: 500\ \text{STB/D} \le \alpha_1 \le 1000\ \text{STB/D}$$

$$1160\ \text{PSIA} \le \alpha_2 \le 1400\ \text{PSIA}$$

$$2\ \text{months} \le \alpha_3 \le 6\ \text{months}$$

where $\underline{\alpha} = \{\alpha_1, \alpha_2, \alpha_3\}$ is a set of process' control variables, α_1, α_2 and α_3, which are the target oil production rate, maximum BHP of the producers, and length of the water cycle time, respectively. Then

$$\mu = \frac{1}{N_t}\sum_{i=1}^{N_t} f_i \tag{16}$$

$$\text{and } \sigma = \sqrt{\frac{1}{N_t}\sum_{i=1}^{N_t}(f_i - \mu)^2} \tag{17}$$

μ and σ are the mean and standard deviation of N_t = 3000 reservoir realisations of the uncertainties, respectively, on which the optimisation under uncertainty routine was performed on.

3.6 The non-dominated sorting algorithm

The ranking of the solutions of the robust optimisation routine was performed to show their level of optimality. The non-dominated sorting algorithm (NSA) was applied to the *"pseudo"* two-objective optimisation problem where the objectives would be maximising the mean, μ and minimising the risk/standard deviation, σ. The ranks of the solutions were depicted as individual Pareto fronts. Three-dimensional plots of the engineering variables of the solutions were also made to show the correlations and any other trends between the solutions of each Pareto front.

A summary of the methods applied in this study is presented in Fig. 11.

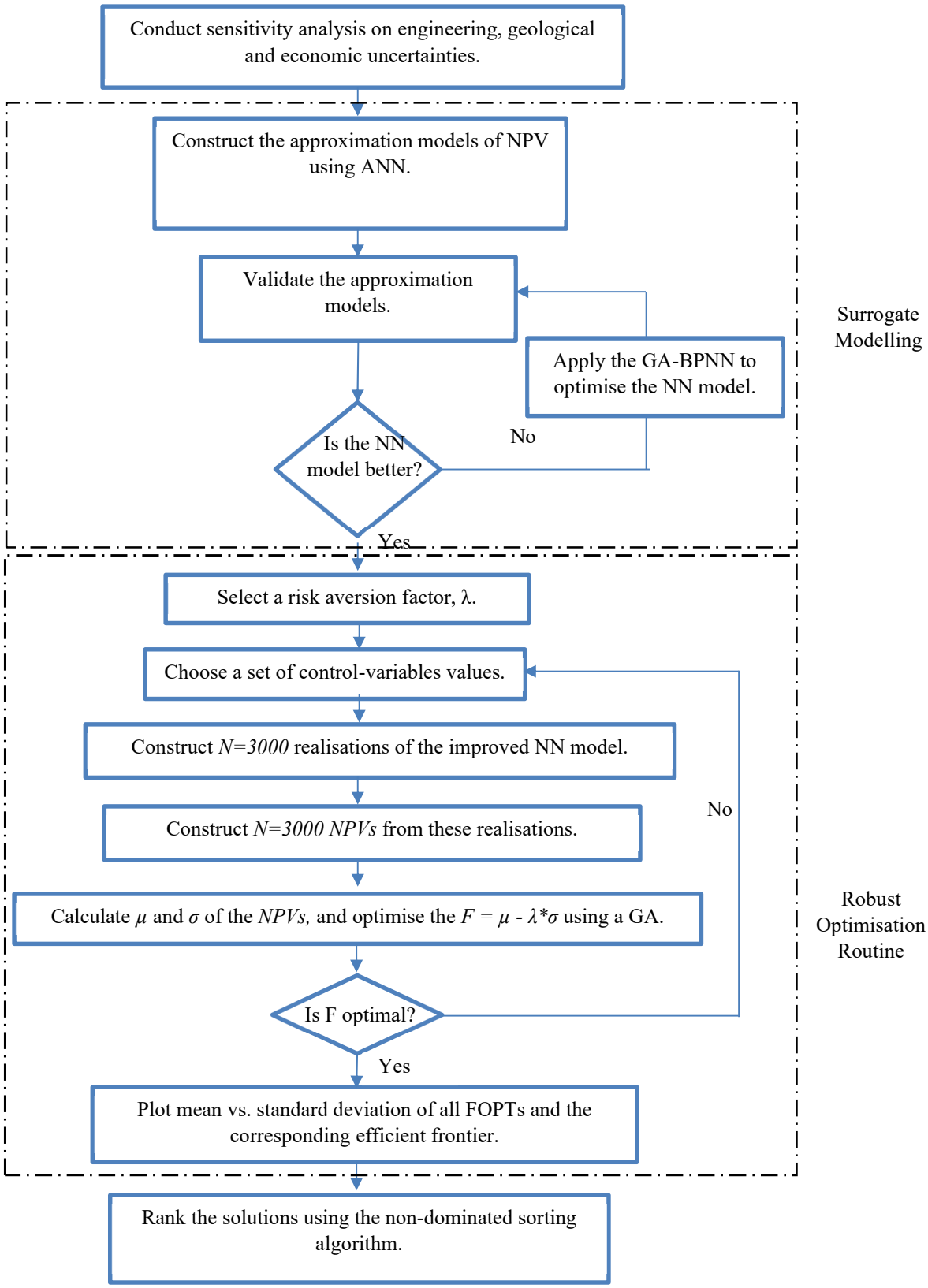

Fig. 11: Workflow for the robust optimisation under geological and economic uncertainties.

4 Results and Discussion

4.1 Optimisation Results

The results of the NO and RO routines are presented in this section. The computational costs of each run in a 3.60 GHz computer processor are shown in Table 10.

Table 10: Computational costs of proxy model evaluation and full reservoir simulation

Scenario	CPU cost
Full-physics numerical model run	30 mins
Surrogate model run	10 s
Nominal optimisation scenario using the NN model	15 s
Robust Optimisation using the surrogate model	120 s

4.1.1. Nominal Optimisation using the Genetic Algorithm

Table 9 presents the genetic algorithm operators applied in the nominal optimisation routine. The specified mutation probability ensured that the algorithm sampled a broader search space and was not struck at a local minimum value. The specified tolerance function tells the algorithm the required difference between the new and existing optimal values, and the optimisation routine is terminated when the defined value is achieved. Fig. 11 shows a plot of the best and mean fitness values of each generation/iteration. The mean NPV improved with each iteration until it reached its best value at the 24th generation.

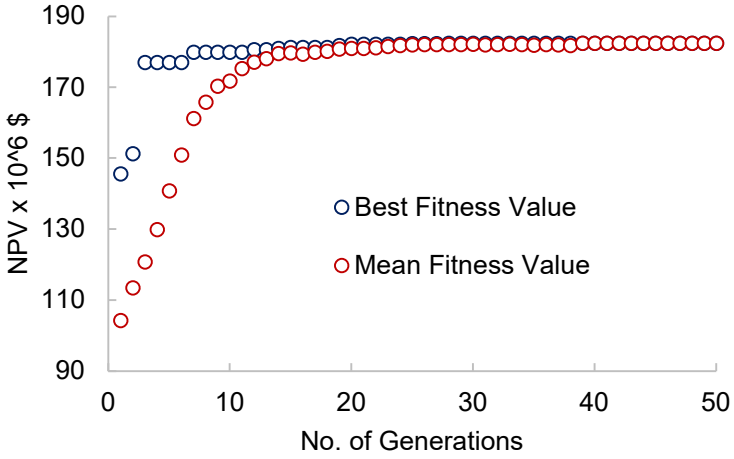

Fig. 11: Result of the NO routine.

The optimal operation parameters are presented in Table 11. The NPV of the project is 182.46 x 10^6 USD when the target oil production rate, maximum bottom-hole pressure of the producers, and the water cycle length were 1000 stb/d, 1160 psia and two months, respectively. A confirmation test was conducted to validate the results obtained by applying the optimal solution to a full-physics simulation of the WAG injection and then computing the NPV of the project. Using the numerical simulator resulted in an NPV of 182.4 x 10^6 USD, representing a relative percentage error of 0.03%, implying that the proxy-predicted value agreed with the simulation result.

Overall, the optimum target BHP of the producers corresponded to the lowest possible pressure required to guarantee a maximum pressure drawdown and miscibility. The optimum water injection cycle time was two months, the minimum value of water injection cycle time, and a longer duration of gas injection. On the other hand, the optimum target oil production rate corresponded to the maximum possible value of this parameter applied in the optimisation.

Table 11: Optimum control variables from the nominal optimisation routine.

Variable	Units	Optimum Values
Target Oil Rate	STB/D	1000
Maximum BHP of the producers	PSIA	1160
Length of Water Cycle Time	Months	2
Net Present Value, NPV	MM$	182.46

4.1.2. Robust Optimisation of the value of the WAG project

The plot of the reward versus the risk of the optimisation runs for each λ are presented in Fig. 12(a), with the sub-plots (Fig. 12(b) – (e)) showing the plots for each risk-aversion factor. Each data point represents $\mu(\underline{\alpha})$ vs $\sigma(\underline{\alpha})$ for a unique set of engineering, $\underline{\alpha}$, obtained from the GA and 3000 realisations of the uncertainties.

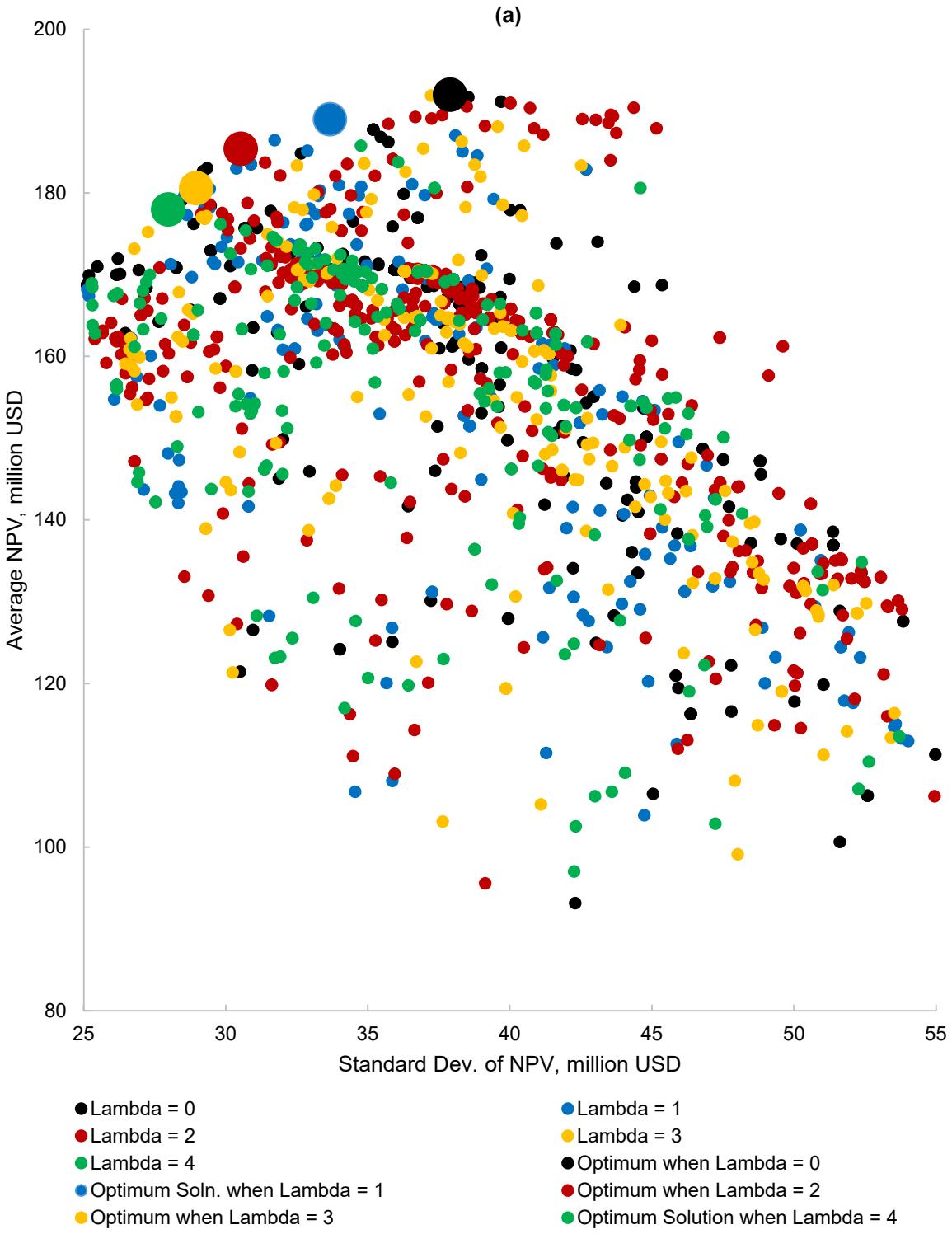
(a)
200
180
160
140
120
100
80
Average NPV, million USD
25
30
35
40
45
50
55
Standard Dev. of NPV, million USD
Lambda = 0
Lambda = 1
Lambda = 2
Lambda = 3
Lambda = 4
Optimum when Lambda = 0
Optimum Soln. when Lambda = 1
Optimum when Lambda = 2
Optimum when Lambda = 3
Optimum Solution when Lambda = 4

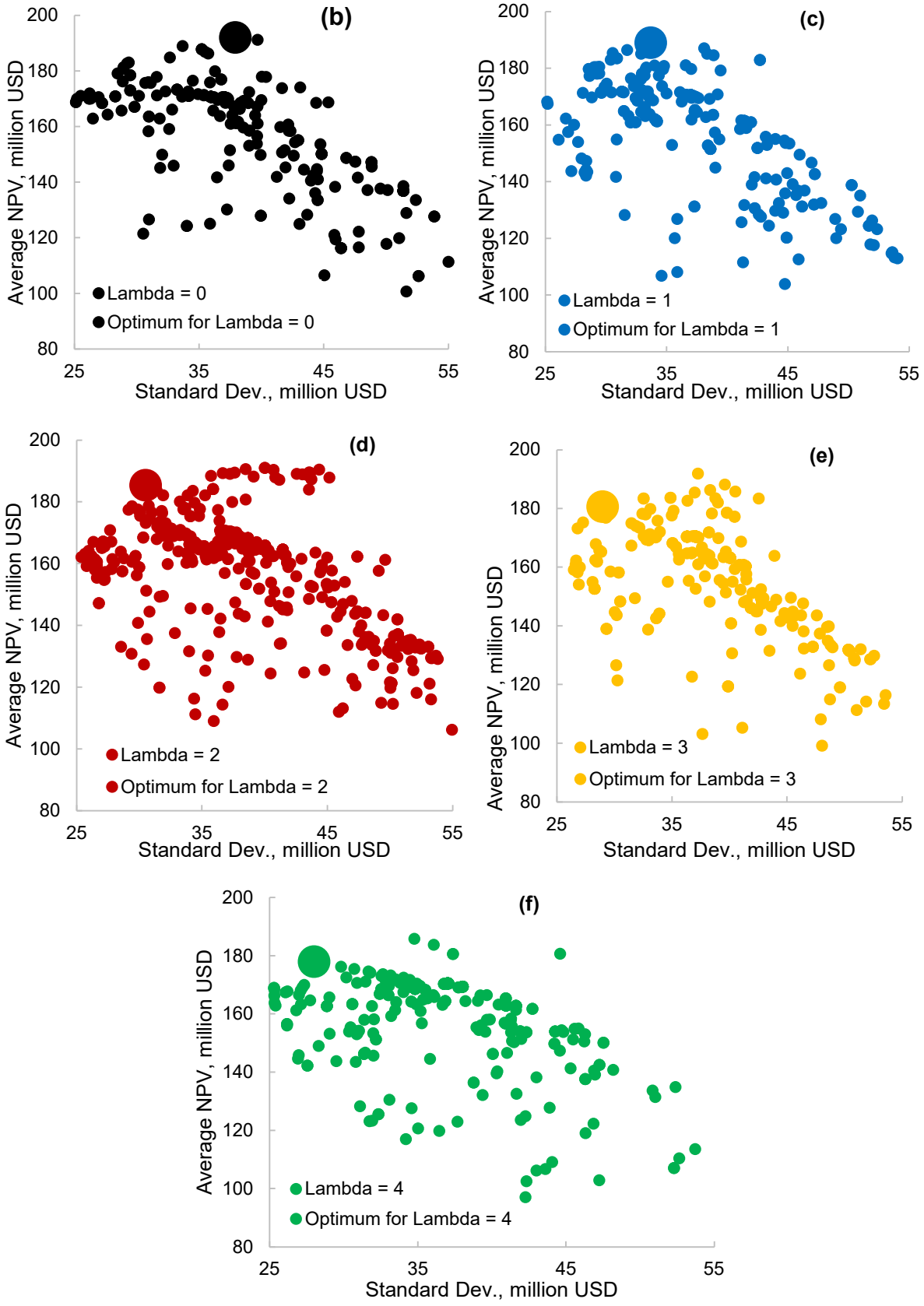

Fig. 12: (a) The efficient frontier and mean-standard deviation plot for the robust optimisation of the pilot WAG injection project, and the subplots for λ = (b) 1 (c) 2 (d) 3 (e) 4 (f) 5

These large markers (representing the optimal solutions) and other solutions formed a convex hull known, as the efficient frontier as shown in Fig. 12(a). Moving from left to right on the standard deviation axis (which represents an increase in the associated risk) shows a corresponding increase in the values of the NPV as the aversion to risk decreases. Other data points shown under the efficient frontier are inferior non-optimal solutions obtained from the optimisation routine.

The results of the robust optimisation routine are presented in Table 12. At a confidence level of 50% (when λ=0), the mean NPV was 192 million USD with a corresponding risk of 37.89 million USD. This means there is a 50% probability that the NPV would be at least this value, which was 5.23% higher than the value of the uncertainty-free optimisation. An increase in the risk-aversion factors led to an increase in the engineer's confidence in the optimisation results but with a corresponding decrease in NPVs. At λ = 1.0, i.e., 84.13% confidence, the NPV would be 154.85 million USD or higher with an associated risk of at least 30.528 million USD.

As λ or confidence increased, the reward decreased with a corresponding decrease in the associated risk. For example, at λ = 4.0, the value of the WAG injection project was 65.98 million USD, i.e., there was a 99.99% confidence level that NPV would be this value or higher with a risk of 27.99 million USD, representing a decrease of 63.84% from the value derived from the nominal optimisation. In summary, the gains/losses of the robust optimisation over the NO scenario were observed to be very significant, particularly as the risk aversion increased.

Table 12: The results of the robust optimisation.

λ	Function Optimized	σ (10^6 \$)	μ (10^6 \$)	Optimized NPV, F (10^6 \$)	Gains over the NO case (%)
0.0	$F = \mu - 0.0\sigma$	37.89	192	192	+5.23
1.0	$F = \mu - 1.0\sigma$	30.53	185.38	154.85	-15.13
2.0	$F = \mu - 2.0\sigma$	33.67	188.97	121.63	-33.34
3.0	$F = \mu - 3.0\sigma$	30.53	185.38	93.79	-48.60
4.0	$F = \mu - 4.0\sigma$	27.99	177.94	65.98	-63.84

Table 13 presents the optimal engineering parameters obtained from the robust optimisation routine. Depending on the engineer's tolerance to risk, they can apply any of the results. These solutions show that a higher target oil production rate and the lowest possible BHP of the producers that would guarantee the flood's miscibility were desirable for maximising the NPV of the WAG flood. Generally, the lowest possible BHP that sustains the miscibility of the flood was preferential as this assures a larger pressure drawdown and, therefore, a higher oil production. However, the NPV of the flood was also clearly dependent on the length of the water cycle time as this parameter is 5.4, 4.95, 4.5, 5.36, and 5.4 months when λ = 1, 2, 3, 4, and 5, respectively. The oil rates, BHPs and the water cycle time obtained were the target controls that the production engineer would apply to optimise the value of the project.

Table 13: The optimal engineering variables from the robust optimisation

Confidence level	Target Oil Production Rate (STB/D)	Max. Producers' BHP (psia)	Length of Water Cycle (Months)
50.0%	1000	1160	5.4
84.13%	1000	1162.7	4.95
97.72%	1000	1160	4.5
99.86%	1000	1160.2	5.36
99.99%	1000	1160.2	5.4

A three-dimensional scatter plot of the control parameters generated and evaluated by the GA as it searches for the optimal solution is shown in Fig. 13. A clustering of the data points was observed for some lambda values (λ = 0.0, 3.0, and 4.0). Other points indicate the optimal solutions when λ = 1.0 and 2.0 and the non-optimal solutions generated by the genetic algorithm. The level of optimality of these solutions can be better described using the non-dominated sorting algorithm.

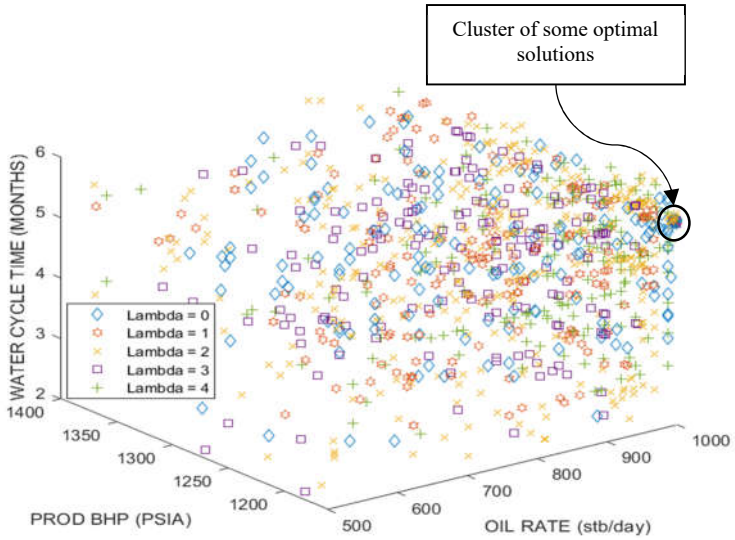

Fig. 13: 3D plot of the solutions of the robust optimisation.

4.2 Non-Dominated Sorting

Fig. 14 shows the results when the non-dominated sorting algorithm was used to sort the solutions of the robust optimisation. Six Pareto fronts of the solutions are displayed, where the first Pareto front, rank 1, represents the solutions on the efficient frontier, which are superior to the solutions of other ranks. If these models are neglected, then a new front, Rank 2, would be obtained which is, in turn, superior to the models in Rank 3. The outcome of this procedure shows each solution's different scales of optimality and presents valuable information for decision-making and reduction of its associated risk(s) to the optimiser or production engineer.

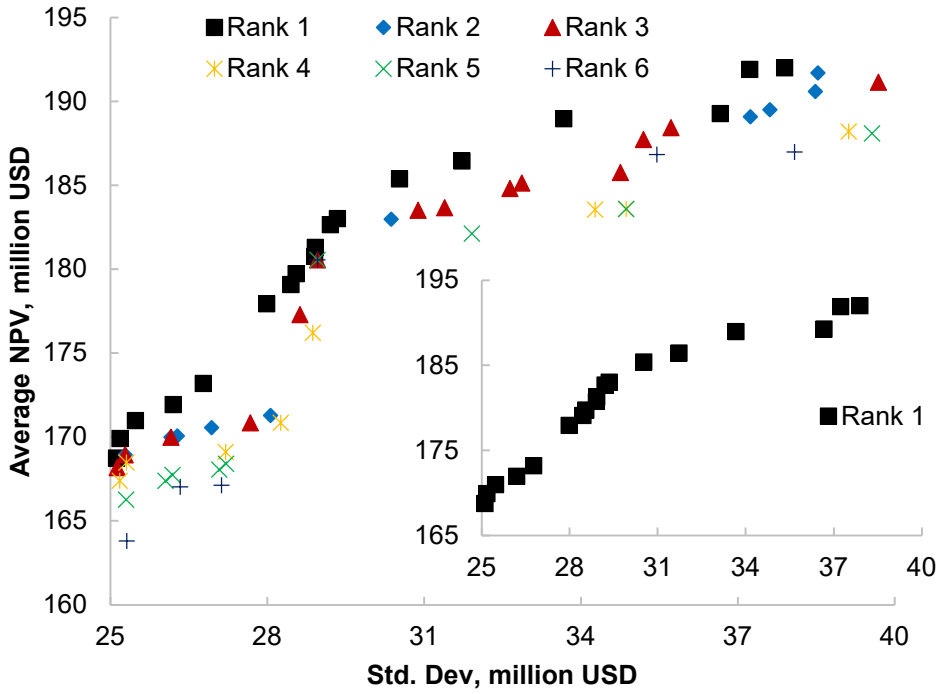

Fig. 14: Ranking the optimisation routine's mean vs standard deviation plots showing the different Pareto fronts. The inset Fig. shows the Pareto in front of Rank 1.

Figs. 15(a) and (b) show the engineering variables of the Pareto fronts and that of the first rank, respectively, in a 3-D space. Like Fig. 16, they depict the levels of optimality of the optimisation solutions. For each front, it was observed that the data points shown in Fig. 18(a) move from right to left as we move from left to right on the Pareto fronts, shown in Fig. 17. We focused on the first Pareto front to outline this trend, as shown in Fig. 18(b). Thus, depending on the risk tolerance of the reservoir engineer, applying any of the solutions to the WAG project would result in an optimal NPV of the WAG project.

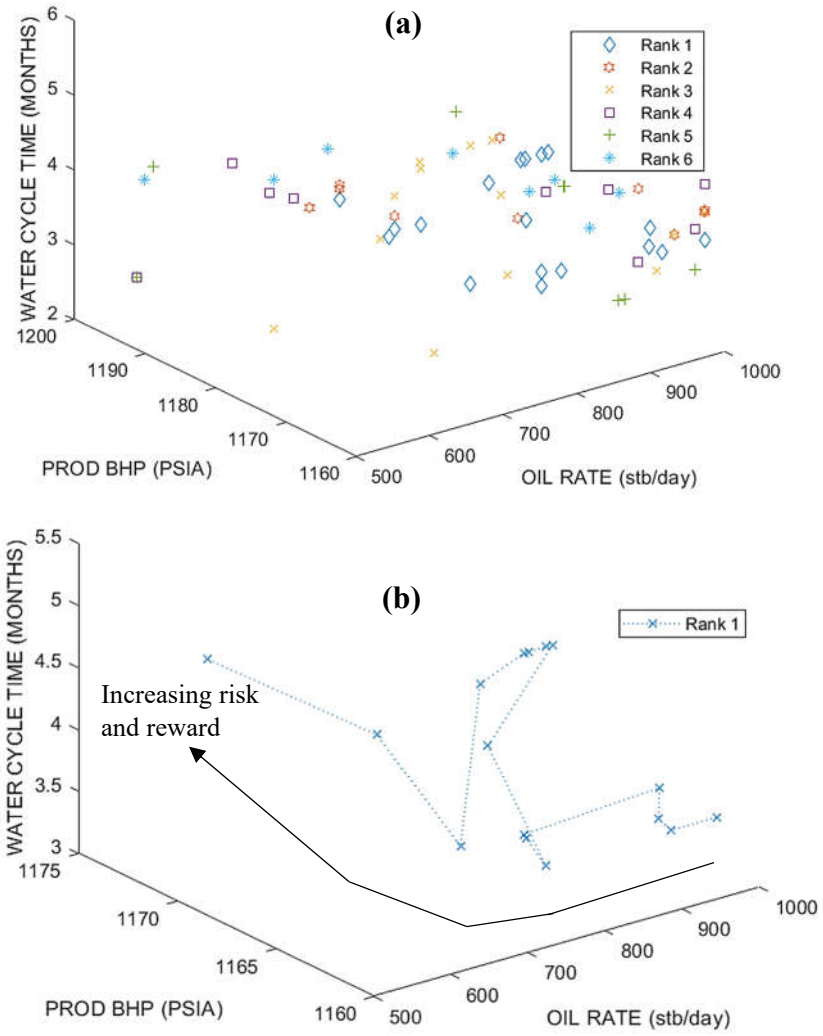

Fig. 15: Plot of the (a) different ranks of solutions obtained during the robust optimisation routine and (b) that of the solutions of the first rank. A general trend in the solutions of rank one is observed as the risks and rewards increase as we move from the right to the left of the 3-D plot.

A series of confirmation tests were performed to validate the results of the robust optimisation by applying the control variables of five solutions on the efficient frontier to full-physics simulations of the WAG injection in 5 realisations of the geological uncertainties and computing the corresponding NPV. Therefore, five NPVs were calculated based on the values of the geological and economic uncertainties for each set of engineering variables. In total, we calculated 25 values of the NPV using the full-physics simulations and 25 values of the NPV using the NN proxy model. We also computed the mean of the five NPVs for each set of engineering variables. The results of this procedure are shown in Fig. 16.

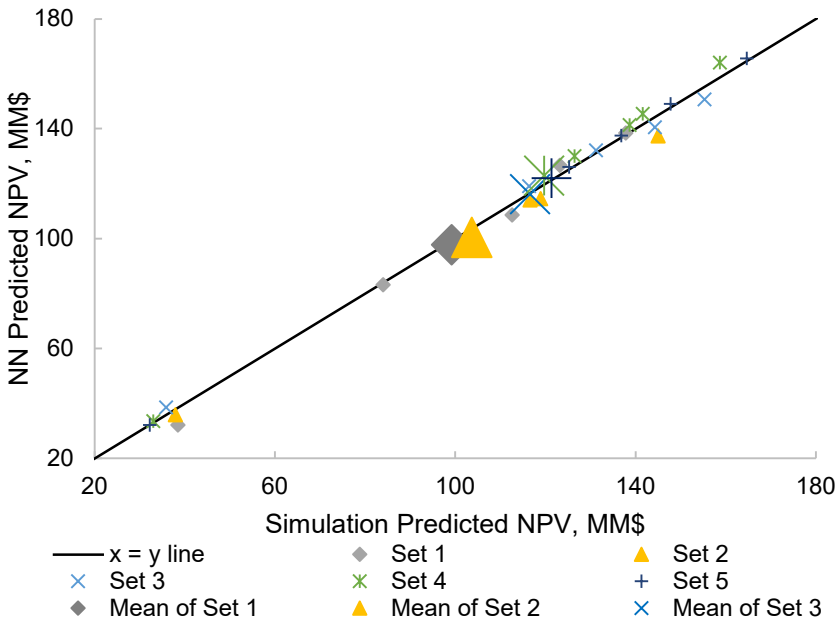

Fig. 16: The cross plot of the simulation-predicted NPV values vs the predictions of the GA-optimised neural network model used to validate the results of the robust optimisation routine. The small icons represent the 25 calculations of the NPV made, where five calculations were made for each set of engineering control variables, while the large icons represent the means of the five NPVs.

Each unique legend represented the result of each set of control variables. The large icons represent the means of the five NPVs calculated for each set of engineering control variables (represented by each unique small icon). Fig. 19 shows that the distribution of the NPV ranged from 35 – 166 x 10^6 USD, which shows the quality of the evaluation as there was a sufficient span of the parameter space. The points on the bottom-left of the plot (i.e., those between 30 – 40 x 10^6 USD) corresponded to the NPVs calculated for the five sets of engineering variables and one set of the economic and geological uncertainties. These uncertainties lie around the low spectrum or the minimum of the parameters' sample space. Other points range between 80 – 166 x 10^6 USD.

The data points are observed to lie around the $x = y$ line, with the R^2 score of all the data points being 0.994, implying that the NN proxy model offers accurate predictions of the performances of the full-physics reservoir simulation model. This also means that the solutions obtained from the proxy-based robust optimisation routine, when implemented for EOR and carbon storage in the reservoir model, will yield accurate predictions of the value of the WAG project.

5 Summary and Conclusions

The numerical simulation and optimisation of the alternating injection of water and CO_2 in turbidite hydrocarbon reservoirs is a computationally expensive process. Using surrogate or proxy models of the desired objective functions can significantly reduce the complexities and costs associated with the full-physics simulations and the optimisation routines.

In this paper, we optimise the Net Present Value of a water-alternating-gas injection project in the presence of uncertainties by applying the Markowitz classical theory to a suitable approximation model of the objective function so that the optimisation routine assessed numerous realisations of uncertainties. We first tested the applicability and accuracies of the neural network modelling technique. To ensure the quality of the resulting

model, we applied a genetic algorithm to improve its performance. Our robust optimisation methodology incorporated petrophysical and economic uncertainties to create better operating strategies for the project that are risk quantified. A summary of the results obtained from the robust optimisation routine showed based on the confidence level of the engineer, an NPV of at least 65.98 x 10^6 USD can be obtained from the project. These solutions were more pragmatic than the result of the deterministic/nominal optimisation (182.46 x 10^6 USD), where uncertainties were not considered. To present the reservoir or production engineer(s) with important information for decision-making and to show different level of optimality. the solutions of the robust optimisation routine were ranked using the non-dominated sorting algorithm.

In summary, in this study, the applicability of data-driven surrogate models for the robust optimisation of the WAG project under geological and economic uncertainties has been demonstrated.

Acknowledgements

The authors wish to acknowledge the Petroleum Technology Development Fund (PTDF) for supporting this study. Schlumberger is also acknowledged for providing the ECLIPSE 300 simulator used in this study.

Data availability

The datasets generated during and/or analysed during the current study are available from the corresponding author on reasonable request.

Funding and/or conflicts of interests/competing interests

The work was funded by the Petroleum Technology Development Fund (PTDF), Grant No.: PTDF/ED/PHD /OP/1348/18.

References

[1] M. D. White, B. J. McPherson, R. B. Grigg, W. Ampomah, and M. S. Appold, "Numerical simulation of carbon dioxide injection in the western section of the farnsworth unit," *Energy Procedia*, vol. 63, pp. 7891–7912, 2014, doi: 10.1016/j.egypro.2014.11.825.

[2] H. Karimaie, B. Nazarian, T. Aurdal, P. H. Nøkleby, and O. Hansen, "Simulation Study of CO2EOR and Storage Potential in a North Sea Reservoir," *Energy Procedia*, vol. 114, no. November 2016, pp. 7018–7032, 2017, doi: 10.1016/j.egypro.2017.03.1843.

[3] Z. Dai *et al.*, "Injectivity Evaluation for Offshore CO2Sequestration in Marine Sediments," *Energy Procedia*, vol. 114, no. November 2016, pp. 2921–2932, 2017, doi: 10.1016/j.egypro.2017.03.1420.

[4] S. Agada, S. Geiger, A. Elsheikh, and S. Oladyshkin, "Data-driven surrogates for rapid simulation and optimization of WAG injection in fractured carbonate reservoirs," *Pet. Geosci.*, vol. 23, no. 2, pp. 270–283, 2017, doi: 10.1144/petgeo2016-068.

[5] K. A. Aghdam and S. S. Ghorashi, "Critical Parameters Affecting Water Alternating Gas (WAG) Injection in an Iranian Fractured Reservoir," vol. 7, no. 3, pp. 3–14, 2017.

[6] V. N. Aghbash and M. Ahmadi, "SPE 153920 Evaluation of CO2-EOR and Sequestration in Alaska West Sak Reservoir Using Four-Phase Simulation Model," *Spe 153920*, p. 16, 2012, doi:

10.2118/153920-MS.

[7] H. Markowitz, “PORTFOLIO SELECTION*,” *J. Finance*, vol. 7, no. 1, pp. 77–91, Mar. 1952, doi: https://doi.org/10.1111/j.1540-6261.1952.tb01525.x.

[8] W. J. Bailey and B. Couet, “Field Optimization Tool for Maximizing Asset Value,” *SPE Reserv. Eval. Eng.*, vol. 8, no. 01, pp. 7–21, 2005, doi: 10.2118/87026-PA.

[9] P. Ogbeiwi, K. Stephen, and A. Akinroola, “Optimisation of Waterflooding under Geological Uncertainties Using an Adaptive Data-Driven Surrogate: Case Study,” vol. 2020, no. 1, pp. 1–5, 2020, doi: https://doi.org/10.3997/2214-4609.202011968.

[10] B. Raghuraman, B. Couët, P. M. Savundararaj, W. J. Bailey, and D. J. Wilkinson, “Valuation of technology and information for reservoir risk management,” *SPE Reserv. Eval. Eng.*, vol. 6, no. 5, pp. 307–316, 2003, doi: 10.2118/86568-PA.

[11] K. Rashid, W. J. Bailey, B. Couet, and D. Wilkinson, “An efficient procedure for expensive reservoir-simulation optimization under uncertainty,” *SPE Econ. Manag.*, vol. 5, no. 04, pp. 21–33, 2013, doi: 10.2118/167261-PA.

[12] P. Ogbeiwi, K. D. Stephen, and A. O. Arinkoola, “Robust optimisation of water flooding using an experimental design-based surrogate model: A case study of a Niger-Delta oil reservoir,” *J. Pet. Sci. Eng.*, vol. 195, no. September, p. 107824, 2020, doi: 10.1016/j.petrol.2020.107824.

[13] S. Agada, S. Geiger, A. Elsheikh, and S. Oladyshkin, “Data-driven surrogates for rapid simulation and optimization of WAG injection in fractured carbonate reservoirs,” *Pet. Geosci.*, vol. 23, no. 2, pp. 270–283, 2017, doi: 10.1144/petgeo2016-068.

[14] W. Ampomah, R. S. Balch, and M. Cathar, “SPE-180084-MS Performance of CO 2 -EOR and Storage Processes Under Uncertainty,” 2016.

[15] W. Ampomah *et al.*, “Optimum design of CO2 storage and oil recovery under geological uncertainty,” *Appl. Energy*, vol. 195, pp. 80–92, 2017, doi: 10.1016/j.apenergy.2017.03.017.

[16] C. A. Dalton, M. B. Broussard, and W. J. Al-Mudhafar, “Proxy-based optimization of hydraulic fracturing design in horizontal wells through CO2 flooding in shale oil reservoirs,” in *51st US Rock Mechanics / Geomechanics Symposium 2017*, 2017, vol. 4, pp. 2718–2726.

[17] T. Simpson, F. Mistree, J. Korte, and T. Mauery, “Comparison of response surface and kriging models for multidisciplinary design optimization,” in *7th AIAA/USAF/NASA/ISSMO Symposium on Multidisciplinary Analysis and Optimization*, American Institute of Aeronautics and Astronautics, 1998.

[18] W. J. Al-Mudhafar, C. A. Dalton, and M. I. Al Musabeh, “Metamodeling via hybridized particle swarm with polynomial and splines regression for optimization of CO2-eor in unconventional oil reservoirs,” *Soc. Pet. Eng. - SPE Reserv. Characterisation Simul. Conf. Exhib. RCSC 2017*, pp. 121–139, 2017, doi: 10.2118/186045-ms.

[19] J. Zhang and A. Taflanidis, “Evolutionary Multi-Objective Optimization under Uncertainty through Adaptive Kriging in Augmented Input Space,” *J. Mech. Des. Trans. ASME*, vol. 142, no. 1, 2020, doi: 10.1115/1.4044005.

[20] K. Cheng and Z. Lu, “Adaptive sparse polynomial chaos expansions for global sensitivity analysis based on support vector regression,” *Comput. Struct.*, vol. 194, pp. 86–96, 2018, doi: 10.1016/j.compstruc.2017.09.002.

[21] S. AlAmeri, S. Agada, A. Elsheikh, S. Geiger, and F. Doster, “Multi-objective Optimization of WAG Injection in Fractured Carbonate Reservoirs under Geological Uncertainty,” *79th EAGE Conf. Exhib. 2017*, no. June 2017, 2017, doi: 10.3997/2214-4609.201701479.

[22] W. Jia, F. Pan, Z. Dai, T. Xiao, and B. McPherson, “Probabilistic Risk Assessment of CO2Trapping Mechanisms in a Sandstone CO2-EOR Field in Northern Texas, USA,” *Energy Procedia*, vol. 114, no. November 2016, pp. 4321–4329, 2017, doi: 10.1016/j.egypro.2017.03.1581.

[23] T. Foroud, A. Seifi, and B. AminShahidi, “Assisted history matching using artificial neural network based global optimization method - Applications to Brugge field and a fractured Iranian reservoir,” *J. Pet. Sci. Eng.*, vol. 123, pp. 46–61, 2014, doi: 10.1016/j.petrol.2014.07.034.

[24] B. M. Negash, A. Vel, and K. A. Elraies, “Artificial neural network and inverse solution method for assisted history matching of a reservoir model,” *Int. J. Appl. Eng. Res.*, vol. 12, no. 11, pp. 2952–2962, 2017.

[25] L. A. N. Costa, C. Maschio, and D. José Schiozer, “Application of artificial neural networks in a history matching process,” *J. Pet. Sci. Eng.*, vol. 123, pp. 30–45, 2014, doi: 10.1016/j.petrol.2014.06.004.

[26] P. C. Silva, C. Maschio, and D. J. Schiozer, “Application of neural network and global optimization in history matching,” *J. Can. Pet. Technol.*, vol. 47, no. 11, pp. 22–25, 2008, doi: 10.2118/08-11-22-TN.

[27] C. Maschio and D. J. Schiozer, “A new optimization framework using genetic algorithm and artificial neural network to reduce uncertainties in petroleum reservoir models,” *Eng. Optim.*, vol. 47, no. 1, pp. 72–86, 2015, doi: 10.1080/0305215X.2013.868453.

[28] G. Villarrubia, J. F. De Paz, P. Chamoso, and F. De la Prieta, “Artificial neural networks used in optimization problems,” *Neurocomputing*, vol. 272, pp. 10–16, 2018, doi: 10.1016/j.neucom.2017.04.075.

[29] S. Jiang, W. Sun, and L. J. Durlofsky, “A data-space inversion procedure for well control optimization and closed-loop reservoir management,” *Comput. Geosci.*, vol. 24, no. 2, pp. 361–379, 2020, doi: 10.1007/s10596-019-09853-4.

[30] I. Jang, S. Oh, Y. Kim, C. Park, and H. Kang, “Well-placement optimisation using sequential artificial neural networks,” *Energy Explor. Exploit.*, vol. 36, no. 3, pp. 433–449, 2018, doi: 10.1177/0144598717729490.

[31] J. You, W. Ampomah, and Q. Sun, “Development and application of a machine learning based multi-

objective optimization workflow for CO2-EOR projects," *Fuel*, vol. 264, no. November 2019, p. 116758, 2020, doi: 10.1016/j.fuel.2019.116758.

[32] A. Golzari, M. Haghighat Sefat, and S. Jamshidi, "Development of an adaptive surrogate model for production optimization," *J. Pet. Sci. Eng.*, vol. 133, pp. 677–688, 2015, doi: 10.1016/j.petrol.2015.07.012.

[33] R. Jin, W. Chen, and T. W. Simpson, "Comparative studies of metamodelling techniques under multiple modelling criteria," *Struct. Multidiscip. Optim.*, vol. 23, no. 1, pp. 1–13, 2001, doi: 10.1007/s00158-001-0160-4.

[34] W. Ampomah *et al.*, "Optimum design of CO2 storage and oil recovery under geological uncertainty," *Appl. Energy*, vol. 195, no. July 2018, pp. 80–92, 2017, doi: 10.1016/j.apenergy.2017.03.017.

[35] W. J. Al-Mudhafar, D. N. Rao, and S. Srinivasan, "Robust Optimization of Cyclic CO2 flooding through the Gas-Assisted Gravity Drainage process under geological uncertainties," *J. Pet. Sci. Eng.*, vol. 166, no. March, pp. 490–509, 2018, doi: 10.1016/j.petrol.2018.03.044.

[36] C. Maschio, C. P. V. de Carvalho, and D. J. Schiozer, "A new methodology to reduce uncertainties in reservoir simulation models using observed data and sampling techniques," *J. Pet. Sci. Eng.*, vol. 72, no. 1–2, pp. 110–119, 2010, doi: 10.1016/j.petrol.2010.03.008.

[37] M. Nait Amar, N. Zeraibi, and K. Redouane, "Optimization of WAG Process Using Dynamic Proxy, Genetic Algorithm and Ant Colony Optimization," *Arab. J. Sci. Eng.*, vol. 43, no. 11, pp. 6399–6412, 2018, doi: 10.1007/s13369-018-3173-7.

[38] A. C. Bertolini, C. Maschio, and D. J. Schiozer, "A methodology to evaluate and reduce reservoir uncertainties using multivariate distribution," *J. Pet. Sci. Eng.*, vol. 128, pp. 1–14, 2015, doi: 10.1016/j.petrol.2015.02.003.

[39] P. Ogbeiwi, K. Stephen, and A. Arinkoola, "A Surrogate-Based Approach to Waterflood Optimisation under Uncertainty," vol. 2020, no. 1, pp. 1–16, 2020, doi: https://doi.org/10.3997/2214-4609.202035076.

[40] Shell, "EP00- Introducing the E & P Business," 2001.

[41] J. C. Echendu and O. O. Iledare, "Progressive Royalty Framework for Oil- and Gas-Development Strategy: Lessons From Nigeria," *SPE Econ. Manag.*, vol. 8, no. 03, pp. 68–77, Jul. 2016, doi: 10.2118/174846-PA.

[42] K. A. Lawal, "An Improved Estimation of the Storage Capacity of Potential Geologic Carbon-Sequestration Sites," *Nigeria Annual International Conference and Exhibition*. p. SPE-150739-MS, 30-Jul-2011, doi: 10.2118/150739-MS.

[43] L. Sun and W. Chen, "Impact of carbon tax on CCUS source-sink matching: Finding from the improved ChinaCCS DSS," *J. Clean. Prod.*, vol. 333, no. November 2021, p. 130027, 2022, doi: 10.1016/j.jclepro.2021.130027.

[44] S. T. McCoy and E. S. Rubin, “An engineering-economic model of pipeline transport of CO2 with application to carbon capture and storage,” *Int. J. Greenh. Gas Control*, vol. 2, no. 2, pp. 219–229, 2008, doi: https://doi.org/10.1016/S1750-5836(07)00119-3.

[45] N. Wei, X. Li, R. T. Dahowski, C. L. Davidson, S. Liu, and Y. Zha, “Economic evaluation on CO2-EOR of onshore oil fields in China,” *Int. J. Greenh. Gas Control*, vol. 37, pp. 170–181, 2015, doi: 10.1016/j.ijggc.2015.01.014.

[46] P. R. Neal, W. Hou, W. G. Allinson, and Y. Cinar, “Costs of CO2 Transport and Injection in Australia,” *SPE Asia Pacific Oil and Gas Conference and Exhibition*. p. SPE-133900-MS, 18-Oct-2010, doi: 10.2118/133900-MS.

[47] A. T. F. S. Gaspar Ravagnani, E. L. Ligero, and S. B. Suslick, “CO2 sequestration through enhanced oil recovery in a mature oil field,” *J. Pet. Sci. Eng.*, vol. 65, no. 3–4, pp. 129–138, Apr. 2009, doi: 10.1016/J.PETROL.2008.12.015.

[48] M. C. Nogueira and D. D. Mamora, “Effect of Flue Gas Impurities on the Process of Injection and Storage of CO2 in Depleted Gas Reservoirs,” *SPE/EPA/DOE Exploration and Production Environmental Conference*. p. SPE-94906-STU, 07-Mar-2005, doi: 10.2118/94906-STU.

[49] National Energy Board of Canada (NEB), “Canada’s Oil Sands, Opportunities & Challenges to 2015: An Update.” Calgary., 2006.

[50] E. P. Anthony and A. Mohan, “Water Management vs. Water Control: Profitability, Not Cost, Driving the Paradigm Change,” *Trinidad and Tobago Energy Resources Conference*. p. SPE-132253-MS, 27-Jun-2010, doi: 10.2118/132253-MS.

[51] F. Tayari, S. Blumsack, R. Dilmore, and S. D. Mohaghegh, “Techno-economic assessment of industrial CO<inf>2</inf> storage in depleted shale gas reservoirs,” *J. Unconv. Oil Gas Resour.*, vol. 11, pp. 82–94, 2015, doi: 10.1016/j.juogr.2015.05.001.

[52] M. A. Cremon, M. A. Christie, and M. G. Gerritsen, “Monte Carlo simulation for uncertainty quantification in reservoir simulation: A convergence study,” *J. Pet. Sci. Eng.*, 2020, doi: 10.1016/j.petrol.2020.107094.

[53] X. Wang, K. van ’t Veld, P. Marcy, S. Huzurbazar, and V. Alvarado, “Economic co-optimization of oil recovery and CO2 sequestration,” *Appl. Energy*, vol. 222, no. April, pp. 132–147, 2018, doi: 10.1016/j.apenergy.2018.03.166.

[54] B. Hill, S. Hovorka, and S. Melzer, “Geologic carbon storage through enhanced oil recovery,” in *Energy Procedia*, 2013, doi: 10.1016/j.egypro.2013.06.614.

[55] K. A. Lawal, “Alternating Injection of Steam and CO_2 For Thermal Recovery of Heavy Oil,” no. August, p. 327, 2011.

[56] A. Kemp and L. Stephen, “The economics of EOR schemes in the UK continental shelf (UKCS),” *SPE Offshore Eur. Conf. Exhib. OE 2015*, no. September, pp. 8–11, 2015.

[57] K. Welkenhuysen, B. Meyvis, and K. Piessens, “A Profitability Study of CO2-EOR and Subsequent CO2Storage in the North Sea under Low Oil Market Prices,” *Energy Procedia*, vol. 114, no. November 2016, pp. 7060–7069, 2017, doi: 10.1016/j.egypro.2017.03.1848.

[58] Bloomberg, “‘Energy and Oil Prices’, www.bloomberg.com/energy, accessed May. 21, 2022.” 2022.

[59] R. Mokhtari, S. Ayatollahi, K. Hamid, and A. Zonnouri, “Co-optimization of Enhanced Oil Recovery and Carbon Dioxide Sequestration in a Compositionally Grading Iranian Oil Reservoir; Technical and Economic Approach,” *Abu Dhabi Int. Pet. Exhib. Conf.*, 2016, doi: 10.2118/183560-MS.

[60] IHS MARKIT, “CO2 EOR Potential in North Dakota,” no. June, pp. 1–101, 2016.

[61] CITA, “CITA (Companies Income Tax) Act Cap C21, LFN 2004 (as amended).” 2004.

[62] PPT, “PPT (Petroleum Profits Tax) Act Cap 354 Laws of the Federation of Nigeria (LFN) 1990.” 1990.

[63] PTDF, “PTDF (Petroleum Technology Development Fund) Act Cap.355 Laws of the Federation of Nigeria (LFN) 1990.” 1990.

[64] ETF, “ETF (Education Trust Fund) Decree No. 7 of 1993, Federal Government of Nigeria.” 1993.

[65] Nigerian Investment Promotion Commission (NIPC), “Investors’ Guide to Nigeria, 5th ed.,” 19-Dec-2010.

[66] C. Yang, C. Card, and L. Nghiem, “Economic Optimization and Uncertainty Assessment of Commercial SAGD Operations,” *Canadian International Petroleum Conference*. p. PETSOC-2007-029, 12-Jun-2007, doi: 10.2118/2007-029.

[67] PIB, “PIB (Petroleum Industry Bill) of 2009 (as amended.” 2009.

[68] E. I. Onwuka, O. O. Iledare, and J. C. Echendu, “Evaluating the Impact of Depreciation Methods and Production Decline Patterns on Deepwater Economics: A Case Study of Nigeria,” *Nigeria Annual International Conference and Exhibition*. p. SPE-163007-MS, 06-Aug-2012, doi: 10.2118/163007-MS.

[69] A. O. Arinkoola, H. M. Onuh, and D. O. Ogbe, “Quantifying uncertainty in infill well placement using numerical simulation and experimental design: case study,” *J. Pet. Explor. Prod. Technol.*, vol. 6, no. 2, pp. 201–215, 2016, doi: 10.1007/s13202-015-0180-z.

[70] P. Ogbeiwi and K. Stephen, “Modelling and Upscaling Unstable Miscible Displacement Processes: Characterisation of Physical Instabilities,” *SPE Europec featured at 82nd EAGE Conference and Exhibition*. p. D041S013R001, 18-Oct-2021, doi: 10.2118/205117-MS.

[71] Ø. Glasø, “Generalized Minimum Miscibility Pressure Correlation,” *Soc. Pet. Eng. J.*, vol. 25, no. 06, pp. 927–934, Dec. 1985, doi: 10.2118/12893-PA.

[72] M. A. Ahmadi, S. Zendehboudi, and L. A. James, “A reliable strategy to calculate minimum miscibility pressure of CO2-oil system in miscible gas flooding processes,” *Fuel*, vol. 208, pp. 117–126, 2017, doi: 10.1016/j.fuel.2017.06.135.

[73] H. Feng *et al.*, “Journal of Petroleum Science and Engineering Assessment of miscibility effect for CO 2 fl ooding EOR in a low permeability reservoir,” *J. Pet. Sci. Eng.*, vol. 145, pp. 328–335, 2016, doi: 10.1016/j.petrol.2016.05.040.

[74] E. J. Spiteri and R. Juanes, “Impact of relative permeability hysteresis on the numerical simulation of WAG injection,” *J. Pet. Sci. Eng.*, vol. 50, no. 2, pp. 115–139, 2006, doi: 10.1016/j.petrol.2005.09.004.

[75] T. H. V. Pham, T. E. Maast, H. Hellevang, and P. Aagaard, “Numerical modeling including hysteresis properties for CO2 storage in Tubåen formation, Snøhvit field, Barents Sea,” *Energy Procedia*, vol. 4, no. April 2008, pp. 3746–3753, 2011, doi: 10.1016/j.egypro.2011.02.308.

[76] H. Shahverdi and M. Sohrabi, “Modeling of cyclic hysteresis of three-phase relative permeability during water-alternating-gas injection,” *SPE J.*, vol. 20, no. 1, pp. 35–48, 2015, doi: 10.2118/166526-pa.

[77] Y. Assef, A. Kantzas, and P. Pereira Almao, “Numerical modelling of cyclic CO2injection in unconventional tight oil resources; trivial effects of heterogeneity and hysteresis in Bakken formation,” *Fuel*, vol. 236, no. August 2018, pp. 1512–1528, 2019, doi: 10.1016/j.fuel.2018.09.046.

[78] S. Agada, C. Kolster, G. Williams, H. Vosper, N. Macdowell, and S. Krevor, “Sensitivity Analysis of the Dynamic CO 2 Storage Capacity Estimate for the Bunter Sandstone of the UK Southern North Sea,” *Energy Procedia*, vol. 114, pp. 4564–4570, 2017, doi: 10.1016/j.egypro.2017.03.1575.

[79] Mathworks Inc, “MATLAB.” 2019.

[80] O. D. Arigbe, M. B. Oyeneyin, I. Arana, and M. D. Ghazi, “Real-time relative permeability prediction using deep learning,” *J. Pet. Explor. Prod. Technol.*, vol. 9, no. 2, pp. 1271–1284, 2019, doi: 10.1007/s13202-018-0578-5.

[81] G. Chen *et al.*, “The genetic algorithm based back propagation neural network for MMP prediction in CO2-EOR process,” *Fuel*, vol. 126, pp. 202–212, 2014, doi: 10.1016/j.fuel.2014.02.034.